PRESSURES IN THE STAGNATION REGIONS OF BLUNT BODIES IN THE VISCOUS-LAYER TO MERGED-LAYER REGIMES OF RAREFIED FLOW

By

J. Leith Potter and Allan B. Bailey

von Kármán Gas Dynamics Facility

ARO, Inc.

TECHNICAL DOCUMENTARY REPORT NO. AEDC-TDR-63-168

September 1963

Program Element 62405334/8953, Task 895306

ARNOLD ENGINEERING DEVELOPMENT CENTER

AIR FORCE SYSTEMS COMMAND

UNITED STATES AIR FORCE

NOTICES

PRESSURES IN THE STAGNATION REGIONS OF BLUNT BODIES IN THE VISCOUS-LAYER TO MERGED-LAYER REGIMES OF RAREFIED FLOW

By

J. Leith Potter and Allan B. Bailey

von Kármán Gas Dynamics Facility

ARO, Inc.

a subsidiary of Sverdrup and Parcel, Inc.

FOREWORD

ABSTRACT

Experimental data on pressures in the stagnation regions of hemispherical and flat noses on axisymmetric bodies in rarefied, hypersonic flow are presented. Diatomic and monatomic gases were used in the study, thereby illustrating the effect of molecular structure on the impact pressure. The experiments were conducted with the models in both cold-wall and insulated-wall conditions. It is concluded that impact pressures may be smaller than the corresponding inviscid values, although this reduction may amount to only a few percent. Small influences of wall heat transfer and molecular structure on impact pressure at a given Reynolds number are demonstrated. Pressure distribution on highly cooled, flat and hemispherical noses are predicted with generally acceptable accuracy by theories for inviscid flows. Flow conditions for these experiments were such that the Knudsen number of a full-scale nose having a radius of one foot and moving with hypersonic speed at altitudes of roughly 300,000 ft was duplicated. Thus, this report concerns the viscous-layer to merged-layer regimes of flow at altitudes above Earth where thermochemical reactions in the shock layers of blunt bodies are believed to be essentially frozen.

PUBLICATION REVIEW

This report has been reviewed and publication is approved.

Jay T. Edwards, III
Capt, USAF
Gas Dynamics Division
DCS/Research

Donald R. Eastman, Jr.
DCS/Research

CONTENTS

TABLES

ILLUSTRATIONS

NOMENCLATURE

D	Outside diameter of the impact-pressure probe
d	Orifice diameter
K	Curvature of body nose (Eq. (5))
ℓ	Axial distance along the nozzle, positive downstream
M_∞	Free-stream Mach number
p	Pressure
p_i	Indicated impact pressure
p_o'	Ideal, inviscid impact pressure
p_∞	Free-stream static pressure
R	Characteristic nose dimension
Re_2	Reynolds number based on radius and conditions immediately downstream of a Hugoniot shock (Eq. (10))
R_s	Shock radius of curvature
T_{aw}	Adiabatic recovery wall temperature
T_o	Free-stream total temperature of gas
T_w	Wall temperature
U_∞	Free-stream velocity
u	Velocity tangential to body surface
v	Velocity normal to body surface
x	Distance tangential to body surface $\Big\}$ Fig. 4
y	Distance normal to body surface
γ	Ratio of specific heats
Δ	Shock-layer thickness
δ	Boundary-layer thickness
ϵ	Density ratio across a normal shock $= \rho_\infty / \rho_2$
θ	Angle between the local normal to the surface and the direction of the undisturbed free-stream velocity
λ_∞	Free-stream mean free path
μ	Coefficient of viscosity

μ'	Dilational coefficient of viscosity
μ''	Longitudinal coefficient of viscosity
μ_2	Viscosity based on conditions immediately downstream of a Hugoniot shock
ρ_2	Density immediately downstream of a Hugoniot shock
ρ_∞	Free-stream density

1.0 INTRODUCTION

This report concerns an investigation in the von Kármán Gas Dynamics Facility (VKF), Arnold Engineering Development Center (AEDC), Air Force Systems Command (AFSC), on the impact pressure and pressure distribution in the stagnation region on hemispherical and flat noses of axisymmetric bodies in flow of very low Reynolds number and supersonic or hypersonic free-stream Mach number. In particular, conditions of heat transfer to the body, varying gas molecular structure, and nose geometry are examined. Special effort is made to establish the true state of affairs in the intermediate, low range of Reynolds numbers where there is interest in the question of whether impact pressure may decrease below the level corresponding to high Reynolds numbers. At the lowest Reynolds numbers investigated, it is well established that impact pressure rises above the corresponding value at high Reynolds numbers.

For clarity of expression, the actual impact pressure imposed on a probe is denoted by p_i. The impact pressure that would be indicated by the same probe under otherwise identical conditions except with Reynolds number sufficiently large to preclude any appreciable viscous influence is denoted by p_o'. Hereafter p_o' is referred to as the ideal pressure.

Previously published results of experimental work have established the qualitative behavior of impact pressure at low Reynolds numbers. However, the investigations have not in all cases been as straightforward as one might think. All low-density, continuous tunnels now in operation are small. This characteristic, in combination with the strong, combined influence of Reynolds number and Mach number on nozzle flow in these tunnels, has limited the useful range of Reynolds numbers attainable. Thus, it has often been necessary to determine the ideal impact pressure, p_o', by extrapolation or by bootstrap technique. This is not desirable when errors on the order of one percent are important, although such errors would not have a significant effect on the determination of flow conditions in the tunnel test section on the basis of impact-pressure surveys.

Variations in Mach number following from variations in effective nozzle expansion area caused by changing boundary-layer thickness were present in many experiments. A part of the influence of varying Mach

---

Manuscript received July 1963.

1

number can be eliminated by referring results to a Reynolds number based on conditions immediately downstream of the normal part of the bow shock wave. However, this parameter is very difficult to calculate when the shock wave and boundary layer merge, and in most cases, the effect of this merger is neglected. Considering that closeness to merging is determined by both Mach and Reynolds numbers, the question of Mach number independence deserves further attention. This point is discussed later.

Aside from difficulties arising from limited Reynolds number range and undesirable variations in Mach number, several other points may be raised. The influence of axial pressure gradients has been present in some investigations, and it now appears that this is a factor of consequence in very precise tests if the gradient is large. The body dimension of most significance deserves reexamination in some cases, and it is important to consider the orifice diameter and thermal transpiration as possible factors. The authors have attempted to evaluate and eliminate these errors insofar as they are able.

2.0 DESCRIPTION OF PRESENT EXPERIMENTS

2.1 WIND TUNNEL

The LDH Wind Tunnel (Ref. 1) is a continuous-type, arc-heated, ejector-pumped design. The major components are (1) d-c arc-heater of the constricted, non-rotated arc and non-swirl gas injection type, with a 40-kw power supply, (2) settling section of variable size but normally of 3-in. diameter and 6.25- to 10-in. length, (3) aerodynamic nozzle of varying design with 0.10- to 0.75-in.-diam throat and 2- to 6-in.-diam exit, (4) a tank of 48-in. diameter surrounding the test section and containing instrumentation and probe carrier, (5) interchangeable diffuser, (6) air-ejector of two stages, and (7) the VKF vacuum pumping system. All critical components of the tunnel are protected by back-side water cooling. The two-stage ejector system is driven by air instead of steam because of the ready availability of the former at the tunnel location and the savings in cost.

The working gas normally is nitrogen or argon, although other gases may be used. Photographs of models being tested in argon are shown in Fig. 1. Typical ranges of operating variables with presently available nozzles are given in Tables 1 and 2.

Reservoir conditions have been established on the basis of measurements of total pressure, mass flow rate, and nozzle throat area. The total enthalpy computed from knowledge of these quantities has been verified by calorimetry measurements giving total enthalpy at the nozzle throat directly (Ref. 2).

The test section conditions have been established on the basis of measured or calculated reservoir conditions and determination of the existence of an inviscid core flow along the nozzle plus measurements of impact pressure, local mass flow rate, static pressure, and local total enthalpy (Refs. 1-3). These have been supplemented by measurements of drag and heat transfer which yield indirect verification of the calibration when compared to other experimental and theoretical data. Theoretical analysis of molecular vibrational relaxation (Ref. 4) has been relied on for final interpretation of experimental measurements. On this basis it is considered that molecular vibration is essentially frozen at all stations downstream of the nozzle throat when nitrogen is the medium. Argon is treated as a perfect gas at the enthalpy levels of these experiments.

2.2 PROBES AND MODELS

This report is primarily concerned with three body shapes: flat-nosed, externally chamfered, and hemispherical-nosed ones. The significant dimensions of these probes are listed in Tables 3 and 4. A brief study of "incomplete" hemispherically nosed probes was made, and the significant dimensions are shown in Fig. 10.

A 1.0-in.-diam, water-cooled, flat-nosed, pressure-distribution model was constructed with eight 0.015-in.-diam pressure sensing orifices on the front surface. A series of eight 0.5-in.-diam water-cooled spheres, each having a single 0.052-in.-diam pressure sensing orifice, was used to determine the distribution of pressure over a sphere. The orifices were located at 0, 15, 30, 45, 60, 75, 90, and 100 deg measured from the stagnation point.

The gage used to measure pressure is a diaphragm-type, variable-reluctance, differential-pressure transducer with an operating range of 0.15 psi. This instrument is calibrated at frequent intervals by means of an oil-filled micromanometer and a McLeod gage. A typical calibration yields a linear gage response of 100 counts full scale, for differential pressure ranges in steps of 0.015, 0.0225, 0.030, 0.045, 0.075, 0.105, and 0.15 psi.

3.0 EXPERIMENTAL DATA

3.1 INFLUENCE OF AXIAL, FREE-STREAM FLOW GRADIENT

As mentioned in Ref. 5, testing in flows having axial gradients in the free stream may introduce some difficulties in the interpretation of results, particularly from probes of larger diameter. This problem arises because the bow shock wave of the larger probe is farther up-stream than that of a smaller probe even though the location of the probe relative to the nozzle is the same in each case. Thus, if $dp_i/d\ell$ is negative, as is usual, the larger probe will indicate a higher value of p_i than the smaller probe, even when Reynolds number is not a factor. This can be a source of difficulty when the experimenter is trying to determine the ideal impact pressure, p_o', by testing large probes at higher pressures in the typically small, low-density wind tunnels now in existence.

If it is considered that the impact pressure measured by the probe is that corresponding to the nozzle station where the normal part of the bow shock lies, a correction of the form

$$p_{i_{corr.}} = p_{i_{read}} + \Delta\,(dp_i/d\ell) \tag{1}$$

may be made, provided Δ is known. In the present situation, $dp_o'/d\ell$ was determined from surveys using a relatively small probe compared to the ones requiring a significant correction. (It may be noted that $d^2p_i/d\ell^2$ is very small along the axis of the test section). Then, the shock-layer thickness, Δ, was estimated on the basis of data given in Ref. 6 and other sources listed therein. This information was combined as shown in Eq. (1) to determine a correction when oversize probes and severe axial gradients were involved.

Fortunately, the correction was necessary only when dealing with conditions corresponding to large Reynolds numbers. For lower Reynolds numbers, the shock wave cannot be regarded as a sharp discontinuity, i.e., its location cannot be specified precisely. Also, merging of shock and boundary layers occurs, and shock-layer thickness, Δ, increases to much greater values. These events make it hazardous to attempt a correction of the type under discussion when $Re_2 \lesssim 50$. In all the present data, significant corrections ($\gtrsim 1$ percent) were confined to cases where $Re_2 \gtrsim 50$ for flat-nosed probes. Hemispherical-nosed probes required smaller corrections because of smaller shock-layer thickness.

A special experiment was conducted in order to determine if Δ for a solid body was equal to Δ for an impact-pressure probe of the same

geometry. This equality was confirmed to an experimental accuracy of approximately one percent for $0 \lesssim d/D \lesssim 0.85$ by testing flat-nosed probes in a conventional, supersonic tunnel where $Re_2 \approx 2 \times 10^6$.

To check the validity of the foregoing method, one set of the present data, which includes the largest corrections applied, is shown in Fig. 2. There it will be observed that the data are quite divergent before correction and are in excellent agreement after correction. Those data from large probes having corrections of up to 7 percent are shown to agree with data from smaller probes having corrections as low as 1 percent after application of Eq. (1). Additional confirmation of the correction procedure is represented by Fig. 3 wherein data of the present investigation are compared with corresponding data from Ref. 7. The present data included in Fig. 3 were significantly corrected only when $Re_2 > 50$. The data of Ref. 7 require no correction for axial flow gradients.

On the basis of Figs. 2 and 3, it is believed that the correction applied where necessary to the extreme cases in the present experiments is valid. It has enabled the use of conditions yielding larger Reynolds numbers than would have been possible otherwise, and this in turn has aided in the more precise determination of the ideal impact pressure, p_0'.

3.2 INFLUENCE OF ORIFICE SIZE

It has been shown in Ref. 8 that impact probes tested in hypervelocity gas streams may experience an effect whereby the pressure measured with a probe of fixed outside diameter may vary as the pressure sensing orifice diameter is varied. Specifically, as the orifice size decreased, the measured pressure was shown to decrease when Reynolds numbers were sufficiently low. It has been suggested that this is caused by a thermal transpiration effect occurring across the pressure sensing orifice. It is also possible that viscous effects or other flow phenomena play a part. In the present case, pressures and orifices are large enough that effects associated with orifice Reynolds or Knudsen number apparently can be ignored on the basis of Refs. 5 and 8.

3.3 CORRELATION PARAMETERS

It has been customary for some time to present data concerning viscous fluid phenomena in the stagnation region of blunt bodies as a function of a Reynolds number based on conditions immediately downstream of the normal part of the bow shock wave, or some approximation thereto. When the Mach number independence principle applies,

5

a suitable Reynolds number alone is adequate for many correlations of blunt-body viscous flow phenomena. However, data corresponding to significantly different shock density ratios are considered later, and it is desirable to review the roles of both shock Reynolds number and density ratio in the present case.

The applicable Navier-Stokes equations offer the needed information, but the difficulties of solving these equations are well known. In order to avoid losing sight of the basic factors in the problem, simplified forms of the equations and straightforward solutions are much to be desired. This means that some approximations must be accepted with the hope that the main features of the flow are not obscured thereby.

Based on the assumption of a thin shock layer, Ho and Probstein (Ref. 9) present simplified Navier-Stokes equations for the problem at hand. The admissibility of the thin shock layer concept has been challenged, but it now appears that this concept is fully adequate for purposes of examining the relevant flow parameters (Ref. 10).

Following Ref. 9, considering only the stagnation streamline, and using the boundary-layer coordinate system sketched in Fig. 4, it may be shown that

$$\rho v \ \partial v / \partial y = -(\partial / \partial y) \ (p - \mu'' \ \partial v / \partial y - E) \tag{2}$$

where, for constant gas properties,

$$E = 2 \left(\mu' + \mu/3 \right) \ \partial u / \partial x \tag{3}$$

If it is assumed that the dilational coefficient of viscosity, μ', is zero and the longitudinal coefficient of viscosity, μ'', is $4\mu/3$, then Eqs. (2) and (3) combine to give

$$\rho v \ \partial v / \partial y = -(\partial / \partial y) \ [p - \mu \ \partial v / \partial y - (\mu/3) \ (2 \ \partial u / \partial x + \partial v / \partial y)] \tag{4}$$

The continuity equation from Ref. 9, with constant density assumed, yields

$$2 \ \partial u / \partial x + \partial v / \partial y + 2 \, K v = 0 \tag{5}$$

where K denotes the curvature of the body, e. g., $K = 1/R$ for a spherical segment. Substituting Eq. (5) in Eq. (4) leads to the result,

$$\rho v \ \partial v / \partial y = -(\partial / \partial y) \ [p + \mu \, (2 \ \partial u / \partial x + 8 \, K v / 3)] \tag{6}$$

If the shock wave is regarded as a Hugoniot shock, total pressure immediately downstream of the shock is the ideal impact pressure, p_o'. Furthermore, at a distance from the body, y, on the order of the

6

boundary-layer thickness, $\partial u/\partial x$ approaches the Newtonian value while the y-component of velocity, v, approaches zero. At the body surface, it is assumed that the no-slip condition exists. Thus, with these assumed boundary conditions, if y = 0 and y = δ are the respective inner and outer limits of integration of Eq. (5) and if μ = const. = μ_2, it is seen that

$$p_i/p_0' \simeq 1 + \mu_2 (2 \, \partial u/\partial x)_\delta / p_0' \qquad (7)$$

For a hemisphere, setting R_S = R, Newtonian theory without the centrifugal correction gives (Ref. 11)

$$(\partial u/\partial x)_\delta = (2 \epsilon)^{1/2} U_\infty/R \qquad (8)$$

and, for a flat-nosed body (Ref. 12),

$$(\partial u/\partial x)_\delta = 4 U_\infty [2 \epsilon (1 - 0.5 \epsilon)]^{1/2} /(3 \pi R) \qquad (9)$$

Substituting Eqs. (8) and (9) in Eq. (7), and setting

$$p_0' = \rho_\infty U_\infty^2 (1 - \epsilon/2)$$

and

$$Re_2 = \rho_\infty U_\infty R/\mu_2 \qquad (10)$$

leads to the approximate results,

$$p_i/p_0' \simeq 1 + 2 (2\epsilon)^{1/2} /Re_2 \qquad (11)$$

for the hemisphere, and

$$p_i/p_0' \simeq 1 + (8/3\pi) (2\epsilon)^{1/2} /Re_2 \qquad (12)$$

for the flat nose.

The foregoing exercise was included because it brings to light the approximate role of the shock density ratio as well as the Reynolds number based on conditions downstream of the normal part of the bow shock wave. It should be remembered that Eqs. (11) and (12) are based on hypersonic-flow, strong-shock approximations and the assumption of a constant-property shock layer. Similar results could be obtained by use of the Hugoniot shock conditions as the outer limits of integration, but the purpose is served by the relations already given.

Following from Eqs. (11) and (12), the experimental data are presented in the form p_i/p_0' versus $Re_2 (\rho_2/\rho_\infty)^{1/2}$. Data for a given ratio of T_w/T_0 and nose shape should be reasonably well correlated by use of these parameters. One example of the improvement effected through use of the parameter $Re_2 (\rho_2/\rho_\infty)^{1/2}$ is illustrated by comparing Figs. 5 and 6. Although the improvement is not spectacular, it is significant.

The appearance of the density ratio as shown in Eqs. (11) and (12) also has been indicated in a study by Matthews (Ref. 7) who did not use it in presenting his experimental data. Although Eqs. (11) and (12) are not badly in error in a quantitative sense, it will be noted that the values of p_i/p_0' less than unity are not predicted, partly because of the assumed Hugoniot shock.

3.4 RAREFIED SHOCK-LAYER REGIMES

Following the criteria of Probstein (Ref. 14), regimes of rarefied flow represented by the data presented herein are identified in terms of the parameter derived in the last section. The relevant definitions in terms of Knudsen numbers for a highly cooled, hemispherical nose are given in the first column and the interpretation applied to the qualitative relations is given in parentheses, as follows:

$$\text{Viscous layer} \text{ - - - - - - - - - - } \lambda_\infty/R \ll \epsilon^{1/2} \quad (0.01-0.03)$$

$$\text{Incipient-merged layer} \text{ - - - - - } \lambda_\infty/R \ll 1 \quad (0.03-0.1)$$

$$\text{Fully merged layer} \text{ - - - - - - - } \lambda_\infty/R < 1 \quad (0.1-1)$$

$$\text{Transitional Flow} \text{ - - - - - - - } \lambda_\infty/R \simeq 1 \quad (1)$$

Inasmuch as the shock-layer thickness, Δ, was used as the characteristic length in deriving the relations given above for the hemisphere, where it was assumed that $\Delta \simeq R\epsilon$, one may approximately convert these relations to apply to flat-nosed bodies by observing that

$$\Delta \text{ Flat-nose } \simeq 3 \Delta \text{ Hemisphere}$$

if effects arising from differences in γ are neglected. Therefore, using a factor of 3 in the relations given for the hemisphere shows that rarefied flow influences are deferred to roughly three times higher Knudsen numbers for flat-nosed bodies.

These Knudsen numbers may be related to $Re_2 (\rho_2/\rho_\infty)^{1/2}$ on the basis of a hypersonic, strong-shock flow model, resulting in

$$Re_2 (\rho_2/\rho_\infty)^{1/2} \simeq C/(\lambda_\infty/R)$$

with

$$C \simeq 8.6 \quad \text{for} \quad \gamma = 1.400$$

and

$$C \simeq 5.8 \quad \text{for} \quad \gamma = 1.667$$

Thus, in terms of the present parameter, the very approximate relations follow:

| Regime | γ | Approximate Maximum $Re_2 \, (\rho_2/\rho_\infty)^{1/2}$ | |
		Hemispherical Nose	Flat-Nose
Viscous layer	1.400	900	300
Viscous layer	1.667	600	200
Incipient-merged layer	1.400	300	100
Incipient-merged layer	1.667	200	70
Fully merged layer	1.400	90	30
Fully merged layer	1.667	60	20
Transitional flow	1.400	9	3
Transitional flow	1.667	6	2

It is obvious that these definitions are arbitrary to a degree, but it is believed helpful to connect the descriptive definitions of the flow regimes with the data to be shown later. No one should attach undue importance to the particular numerical ranges given in the foregoing table.

4.0 RESULTS AND DISCUSSION

4.1 IMPACT PRESSURE

4.1.1 Flat-Nosed Probes at Adiabatic Recovery Temperature

In connection with the earlier discussion of the influence of axial pressure gradients in the free-stream flow, the new data for flat-nosed probes in nitrogen with $T_w = T_{aw}$ were presented in Fig. 3. In that figure, these data were compared with Matthews' GALCIT data, and excellent agreement was demonstrated. Because of the vast number of data points, no direct comparison is made between the data in Figs. 3 and 6, but the agreement between results for the flat-nosed and externally chamfered probes is also good, in the range of the present data, when the characteristic length, R, is defined as the actual nose radius as shown in the sketches accompanying Table 3. Some investigators have used the radius of the afterbody or stem of externally chamfered probes as the characteristic length, but it seems clear that the lip radius is more significant.

One purpose of these experiments was the comparison of results from diatomic and monatomic gases with ratios of specific heats, γ,

equal to 1.400 and 1.667, respectively. The first of these comparisons is presented in Figs. 3 and 7. The flat-nosed probe in monatomic gases returned values of p_i/p_o' that dip to lower values and rise later as $Re_2 (\rho_2/\rho_\infty)^{1/2}$ decreases when compared to the diatomic gas. However, the difference which is attributable to the changed molecular structure of test gas is small, p_i/p_o' being approximately two percent lower in the monatomic gases when merging of shock and boundary layers occurs.

4.1.2 Externally Chamfered Probes at Adiabatic Recovery Temperature

The externally chamfered probe configuration was tested only in nitrogen gas, and this was done mainly to compare it with the flat-nosed shape. Comparison of Figs. 3, 6, and 8 shows that there is little difference between the VKF and GALCIT flat-nosed probe data and the VKF and JPL externally chamfered probe data from air and nitrogen flows.

4.1.3 Hemispherical-Nosed Probes at Adiabatic Recovery Temperature

Comparison of Figs. 9 and 10 demonstrates that the probes whose noses form only a segment of a hemisphere may be treated as hemispherical-nosed shapes when R is defined as shown in Fig. 10, at least for $Re_2 (\rho_2/\rho_\infty)^{1/2}$ in the viscous-layer regime.

To facilitate comparisons between flat- and hemispherical-nosed probes the faired curve fitting the data in Fig. 3 for flat noses is reproduced in Fig. 9. It appears that the dip of p_i/p_o' below unity as well as the later upswing to values above unity occur at roughly three times higher values of $Re_2 (\rho_2/\rho_\infty)^{1/2}$ for the hemispherical nose. Minimum values of p_i/p_o' are only slightly different.

Probstein and Kemp (Ref. 14) have analyzed the viscous and incipiently merged layers on the basis of Navier-Stokes and shock-wave conservation equations simplified according to strong-shock and constant-density shock-layer assumptions. They obtained solutions which, for $T_w = T_{aw}$ and $\gamma = 11/9$, show p_i/p_o' passing from unity to still higher values as Re_2 decreases, i. e., the minimum values less than unity shown in Fig. 9 where $\gamma = 7/5$ are not predicted in Ref. 14 for $T_w = T_{aw}$ and $\gamma = 11/9$. However, such a minimum is calculated for $T_w \ll T_{aw}$ on the basis of Ref. 14.

Results obtained from the present experiments with the hemispherical-nosed probe in argon are presented in Fig. 11. For ease of comparison, curves fitting the data for hemispheres in nitrogen and flat-noses in argon are included. Although the experimental data in this case are not as extensive as one would wish, it appears that the change in gases had the same qualitative effect on the hemisphere as on the flat nose. Namely,

10

the values of p_i/p_0' dip below unity at a somewhat higher value of $Re_2 (\rho_2/\rho_\infty)^{1/2}$ when argon is the medium. The effect of changed nose shape in argon is also consistent with the effect indicated in the case of nitrogen, i. e., the flat nose experiences effects similar to those revealed by the hemisphere, but these effects occur at lower Reynolds numbers for the flat nose.

One of the more interesting aspects of Fig. 11 is the comparison of this experiment and the theory of Levinsky and Yoshihara (Ref. 15) for the hemisphere in argon. The latter used the Navier-Stokes equations, as did Probstein and Kemp, but they did not assume constant density in the shock layer and they integrated the viscous, compressible-flow equations between the body and infinity along the stagnation streamline with the shock included. Unlike Probstein and Kemp, the more recent analysis of Levinsky and Yoshihara shows p_i/p_0' relatively unaffected by T_w/T_{aw}, and it predicts $p_i/p_0' < 1$ in the viscous-layer regime. Figure 11 shows theory and experiment to be in close agreement for $Re_2 (\rho_2/\rho_\infty)^{1/2} \gtrsim 200$ or $Re_2 \gtrsim 100$. This limit is estimated to lie in the incipient-merged-layer regime defined in Section 3.4.

4.1.4 Flat-Nosed, Cooled Probes

The effect of cooling the flat-nosed probe in nitrogen may be seen in Fig. 12. In view of the probable experimental accuracy, it can only be said that cooling had relatively little effect in this case. Figure 13 presents a similar comparison for the flat-nosed probes in argon, and the same conclusion seems warranted. If anything, one would have to conclude that cooling results in a slight diminution of the rarefied-flow effect on p_i/p_0' in the range of Reynolds numbers where $p_i/p_0' < 1$. However, at still lower Reynolds numbers, where $p_i > p_0'$, impact pressure apparently is higher for the cooled body.

Comparison of Figs. 7 and 13 reveals that the effect of changed gas medium is approximately the same regardless of the heat-transfer situation. Specifically, the flat-nose in argon gives lower p_i/p_0' in the viscous-layer to merged-layer regimes. However, the difference is only about two percent.

4.1.5 Hemispherical-Nosed, Cooled Probes

Figure 14 offers evidence which also indicates that cooling has a slight effect on p_i/p_0' in the regimes under discussion, but the small effect shown for cooling is qualitatively similar to that for the flat-nosed probes. In other words, cooling slightly reduces the effect of low Reynolds numbers within the limits of the present data, but not at lower Reynolds numbers where $p_i > p_0'$. The change in nose shape is seen to be

quite consistent with the comparable data in Fig. 9. As indicated in Section 3.4, the flat nose experiences rarefied flow effects at lower Reynolds numbers than the hemisphere.

The final presentation of impact-pressure data in Fig. 15 shows more clearly the apparent limit of validity of the flow model used by Levinsky and Yoshihara. The curve fitting the data for the hemisphere with $T_w = T_{aw}$ (Fig. 11) is not shown because it would lie very close to the theoretical curve of Ref. 15.

Results presented in Fig. 15 reveal that the change from diatomic gas to monatomic gas causes p_i/p_o' to drop to lower values in the regimes of flow studied here. The difference, once again, is only a few percent.

The major influence of nose shape is consistent with all earlier data of this report, the flat nose delaying effects of lowering Reynolds number.

4.1.6 Relation between Impact Pressure and Rarefied-Flow Regimes of Probstein

Based on the necessarily rather indefinite boundaries of the regimes of rarefied flow established in Section 3.4, it is possible to state some qualitative relations between the behavior of impact pressure and these regimes. Inspection of the data presented herein reveals that the ratio p_i/p_o' begins to decrease below unity at values of $Re_2(\rho_2/\rho_\infty)^{1/2}$ which are either somewhat above or below the upper bound of the viscous-layer regime as it is defined herein. Thus, one may say that the onset of rarefied-flow influence on impact pressure corresponds roughly to entrance into the viscous-layer regime, and p_i/p_o' decreases at that time.

The minimum value of p_i/p_o' occurs, in the average case, near the middle of the incipient-merged-layer regime. After this minimum value of p_i/p_o', in terms of decreasing Reynolds number, a reversal in trend occurs and p_i/p_o' increases. The values of p_i/p_o' become greater than unity in the early to middle part of the fully merged-layer regime. The onset of transitional flow finds p_i/p_o' well above unity. Figure 16 is a graphical example of the relation between p_i/p_o' and the regimes of rarefied-flow.

4.1.7 Remarks on Some Older Data

There are two sets of well-known, older data on particular probe geometries which the present authors have reexamined in the light of more recent developments. Inasmuch as the comparison of the older

data and the data of this report involves a reinterpretation of the former, the discussion is relegated to Appendix I.

4.1.8 The Characteristic Length

It is natural to speculate that some characteristic length exists which would correlate data for different nose shapes when used instead of the geometric radius, R, in defining Re_2. Lengths that readily come to mind are shock-wave radius of curvature and shock-layer thickness. Both of these lengths are functions of Mach and Reynolds numbers, and data are insufficient to enable a satisfactory correlation of impact pressures on this basis at this time. However, Appendix II contains a trial result which is of some interest.

4.2 PRESSURE DISTRIBUTION

4.2.1 Flat-Nosed, Cooled Body in Argon

The data for this case presented in Fig. 17 are typical examples of the more extensive investigation. Argon was the gas medium used in this phase of the investigation for reasons having to do with a separate study. There is theoretical evidence that the difference between argon and nitrogen would not be highly significant insofar as distribution of pressure is concerned since one can show, following Probstein (Ref. 12),

$$p/p_i = 1 - 0.18 (x/R)^2 (1 - p_\infty/p_i) \qquad (13)$$

But, for M_∞ large, the influence of M_∞ and γ disappears since $p_\infty \ll p_i$, and one may write

$$p/p_i \approx 1 - 0.18 (x/R)^2 \qquad (14)$$

Actually, the theoretical curve given by Probstein should not be extended far from the stagnation point according to the limit he stated. Nonetheless, his theory is in relatively good agreement with the experimental data all across the nose.

The main purpose of Fig. 17 is to show that there is a consistent but very small effect of viscosity on the distributions after normalizing the data by setting $p_i = p_o'$. Generally, it may be said that the local pressure falls more rapidly toward the shoulder as Reynolds number decreases. However, to within roughly two percent, the inviscid theories (Refs. 12 and 16) agree with the data which extend into the incipient-merged-layer regime.

4.2.2 Hemispherical-Nosed, Cooled Body in Argon

Pressure distribution on the hemispherical-nosed body represented in Fig. 18 follows the modified Newtonian law for $0 < \theta < 70$ deg, i. e.,

$$p/p_i = \cos^2 \theta + (p_\infty/p_i) \sin^2 \theta \qquad (15)$$

Examination of Fig. 18 leads one to believe that, if there is an effect of Reynolds number at all, it is no greater than that exhibited in Fig. 17 and is probably the same qualitatively.

Here again the influence of γ on p/p_i is very weak in hypersonic flows because the last term in Eq. (15) becomes negligible when M_∞ is large.

5.0 CONCLUSIONS

The fundamental conclusions drawn from this study of the pressure in the stagnation regions of hemispherical and flat noses on axisymmetric bodies in rarefied, hypersonic flow follow:

1. Impact pressure ratio, p_i/p_o', on flat-nosed and hemispherical-nosed bodies first decreases below the inviscid value and later rises above it as Reynolds number decreases. This occurs for either cooled or insulated probe surfaces, with cooling seeming to slightly minimize the amount of the decrease in p_i/p_o'. It also occurs in both monatomic and diatomic gases, the minimum of p_i/p_o' being slightly lower in the monatomic gases studied.

2. Hemispherical-nosed bodies experience the effect of rarefied flow on p_i/p_o' at higher values of Reynolds number than flat-nosed bodies in both monatomic and diatomic gases studied.

3. There is no more than approximately three percent difference in p_i/p_o' attributable to differences in gas medium or wall cooling for a given nose shape at a given value of $Re_2 (\rho_2/\rho_\infty)^{1/2}$ throughout the viscous-layer to merged-layer regimes under the conditions studied. Furthermore, the effect of nose shape is small when $Re_2 (\rho_2/\rho_\infty)^{1/2} \gtrless 100$.

4. Analysis based on the Navier-Stokes equations as described by Probstein and Kemp and later refined by Levinsky and Yoshihara is found to be adequate for $Re_2 \gtrless 100$ in the case of the hemisphere. This limit may drop to $Re_2 \gtrless 30$ for flat noses.

5. There appears to be a qualitative relationship between the behavior of impact pressure and Probstein's regimes of rarefied flow. The decreasing trend of p_i/p_o' at intermediate Reynolds numbers seems related to viscous-layer phenomena, whereas the reversal to an increasing trend seems to be related to merged-layer phenomena. Shock thickening may be a basic factor in decreasing p_i.

6. Pressure distributions on highly cooled, flat and hemispherical noses show a discernible but very small effect of reduced Reynolds number, even when Re_2 is as low as 20. Simple, hypersonic theories were found to agree closely with the experimental data.

REFERENCES

1. Potter, J. L., Kinslow, M., Arney, G. D., Jr., and Bailey, A. B. "Initial Results from a Low-Density Hypervelocity Wind Tunnel." Hypersonic Flow Research, Ed. by F. R. Riddell, Academic Press, 1962, pp. 599-624.

2. Arney, G. D., Jr. and Boylan, D. E. "A Calorimetric Investigation of Some Problems Associated with a Low-Density Hypervelocity Wind Tunnel." AEDC-TDR-63-19, February 1963.

3. Boylan, D. E. "An Analysis of Initial Static Pressure Probe Measurements in a Low-Density Hypervelocity Wind Tunnel." AEDC-TDR-63-94, April 1963.

4. Lewis, A. D. and Arney, G. D., Jr. "Vibrational Nonequilibrium with Nitrogen in Low-Density Flow." AEDC-TDR-63-31, March 1963.

5. Bailey, A. B. "Further Experiments on Impact-Pressure Probes in a Low-Density, Hypervelocity Flow." AEDC-TDR-62-208, November 1962.

6. Bailey, A. B. and Sims, W. H. "The Shock Shape and Shock Detachment Distance for Spheres and Flat-Faced Bodies in Low-Density, Hypervelocity Argon Flow." AEDC-TDR-63-21, February 1963.

7. Matthews, Malcolm L. "An Experimental Investigation of Viscous Effects on Static and Impact Pressure Probes in Hypersonic Flow." GALCIT Hypersonic Research Project Memo. No. 44, June 2, 1958.

15

8. Bailey, A. B. and Boylan, D. E. "Some Experiments on Impact-Pressure Probes in a Low-Density, Hypervelocity Flow." Proceedings of the 1962 Heat Transfer and Fluid Mechanics Institute, Ed. by F. E. Ehlers, et al., Stanford University Press, 1962, pp. 62-75.

9. Ho, Hung-Ta and Probstein, R. F. "The Compressible Viscous Layer in Rarefied Hypersonic Flow." Rarefied Gas Dynamics, Ed. by L. Talbot, Academic Press, 1961, pp. 525-552.

10. Cheng, H. K. "The Blunt Body Problem in Hypersonic Flow at Low Reynolds Number." Paper presented at IAS 31st Annual Meeting, January 21-23, 1963. (IAS Paper No. 62-92).

11. Hayes, W. D. and Probstein, R. F. Hypersonic Flow Theory. Academic Press, 1959, p. 161.

12. Probstein, R. F. "Inviscid Flow in the Stagnation Point Region of Very Blunt-Nosed Bodies at Hypersonic Flight Speeds." Brown University, WADC-TN-56-395 (AD 97273), September 1956.

13. Ashkenas, H. Private Communication from Jet Propulsion Laboratory, September 5, 1962.

14. Probstein, R. F. and Kemp, N. H. "Viscous Aerodynamic Characteristics in Hypersonic Rarefied Gas Flow." Journal of the Aerospace Sciences, Vol. 27, No. 3, March 1960, pp. 174-192.

15. Levinsky, E. S. and Yoshihara, H. "Rarefied Hypersonic Flow over a Sphere." Hypersonic Flow Research, Ed. by F. R. Riddell, Academic Press, 1962, pp. 81-106.

16. Gold, R. and Holt, M. "Calculation of Supersonic Flow Past a Flat-Head Cylinder by Belotserkovskii's Method." Brown University, AFOSR TN-59-199 (AD 211-525), March 1959.

17. Sherman, F. S. "New Experiments on Impact-Pressure Interpretation in Supersonic and Subsonic Rarefied Air Streams." NACA TN 2995, September 1953.

18. Enkenhus, K. R. "Pressure Probes at Very Low Density." UTIA Report No. 43, January 1957.

APPENDIX I

REMARKS ON SOME OLDER DATA

Among the most extensive and better-known early data on impact-pressure probes in supersonic flow are the results of investigations by Sherman (Ref. 17) and Enkenhus (Ref. 18). In Ref. 17 the highest value of $Re_2 (\rho_2/\rho_\infty)^{1/2}$ was approximately 400, whereas in Ref. 18 the upper limit was not quite 20. It is apparent that these limitations imposed a severe handicap when the earlier investigators attempted to determine the ideal impact pressure, p_o'. Therefore, to complete the present study, an attempt has been made to reevaluate these early data on the basis that the values of p_i/p_o' in Refs. 17 and 18 at a given value of $Re_2 (\rho_2/\rho_\infty)^{1/2}$ and for a given nose shape would agree with the more recent data which extend to higher Reynolds numbers. There is no nose shape common to both the older and newer data, but the tentative assumption that the externally chamfered and internally chamfered noses are equivalent at the higher Reynolds numbers will be made in order to enable a comparison. (The apparent validity of this assumption is confirmed by Fig. I-2.)

In Fig. 23 of Ref. 17, Sherman gives some limited data on both internally chamfered and source-shaped probes at a nominal Mach number of 4 with $T_w = T_{aw}$. By using the AEDC-VKF and the JPL data of Ref. 13 to fix the value of p_i/p_o' at the higher Reynolds numbers of Sherman's experiments, the form of p_i/p_o' variation with $Re_2 (\rho_2/\rho_\infty)^{1/2}$ for the internally chamfered probes in Sherman's tests can be derived. The results for the internally chamfered probe and the correspondingly adjusted data for the source-shaped probe are shown in Fig. I-1.

Using the internally chamfered probe as a basis for defining p_o', the data contained in the main body of Sherman's report have been reworked, and the results of this are shown in Figs. I-2 and I-3. It will be noted that there is good agreement between the AEDC data for externally chamfered probes and Sherman's data for internally chamfered probes. Also, the degree of agreement between the data for source-shaped probes and the AEDC data for hemispherical-nosed probes is good.

Using the technique described above, Enkenhus' data for externally chamfered probes with $T_w = T_{aw}$ have been recalculated and are shown in Fig. I-4. In this case, Enkenhus' values of p_i/p_o' at his higher Reynolds numbers have been forced to agree with the AEDC and JPL data. It is apparent that good agreement then ensues throughout the Reynolds number range.

The results of this reexamination show that the older and newer data agree in those cases where similar conditions existed if the values of the ideal impact pressures in the older experiments are changed only a few percent. Although it is not possible to state this conclusion with a high level of confidence because of the method that has to be used to obtain this agreement, it appears that some of the inconsistencies that have troubled investigators in the past were perhaps attributable to small experimental inaccuracies caused by the limited range of Reynolds numbers attainable in the older experiments. Within the restrictions of this comparison, it is also suggested that internally and externally chamfered probes yield essentially equivalent impact pressures in the flow regimes studied. Furthermore, to the same extent, there would seem to be little difference between source-shaped and hemispherical-nosed probes.
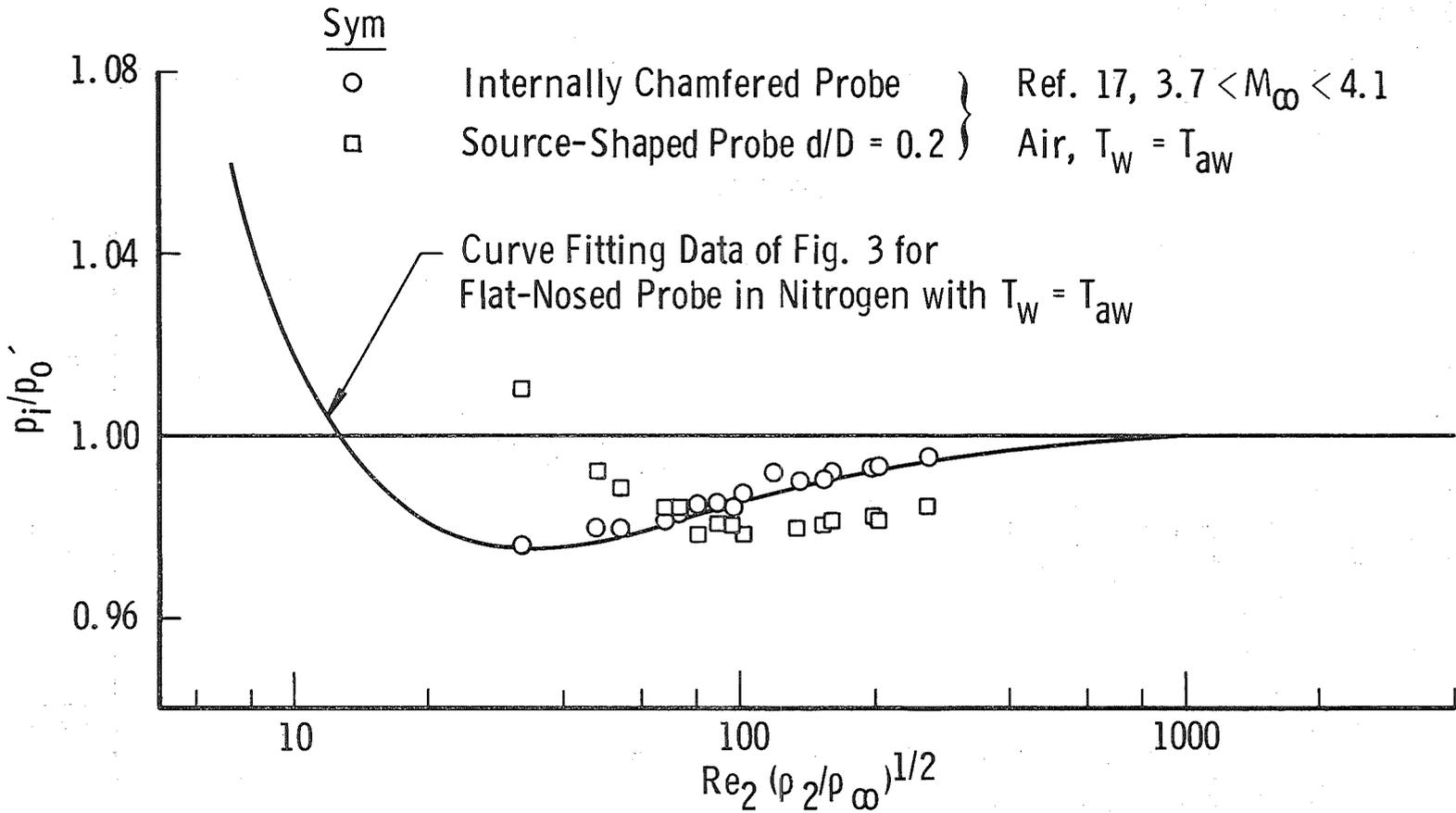
Fig. I-1 Result of Reinterpreting Sherman's Data by Forcing Its Agreement with Newer Data for Externally Chamfered Probes at Higher Reynolds Numbers
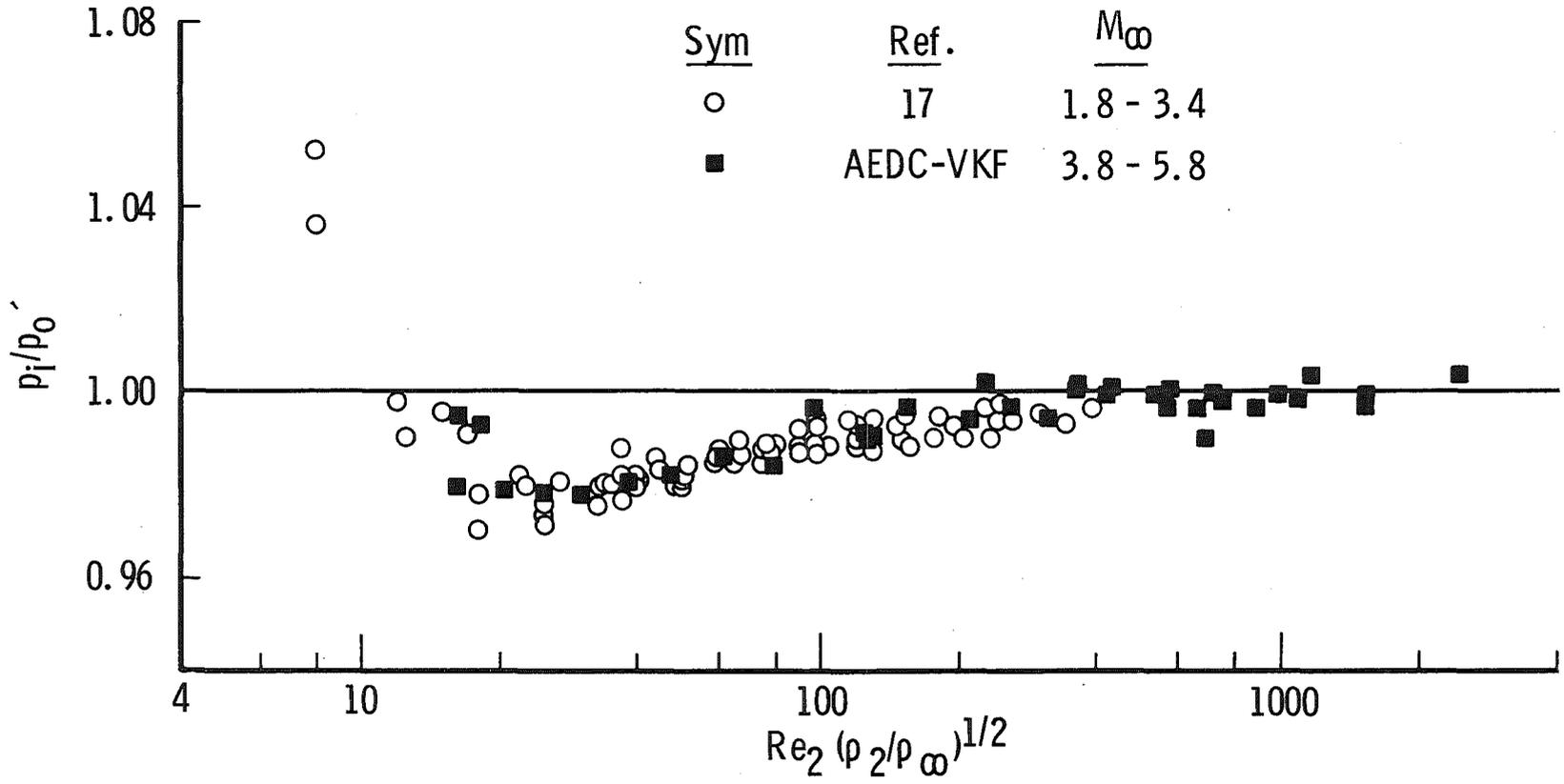
Fig. I-2 Comparison of AEDC-VKF External-Chamfer Probes with Sherman's Internal-Chamfer Probes, $T_w = T_{aw}$
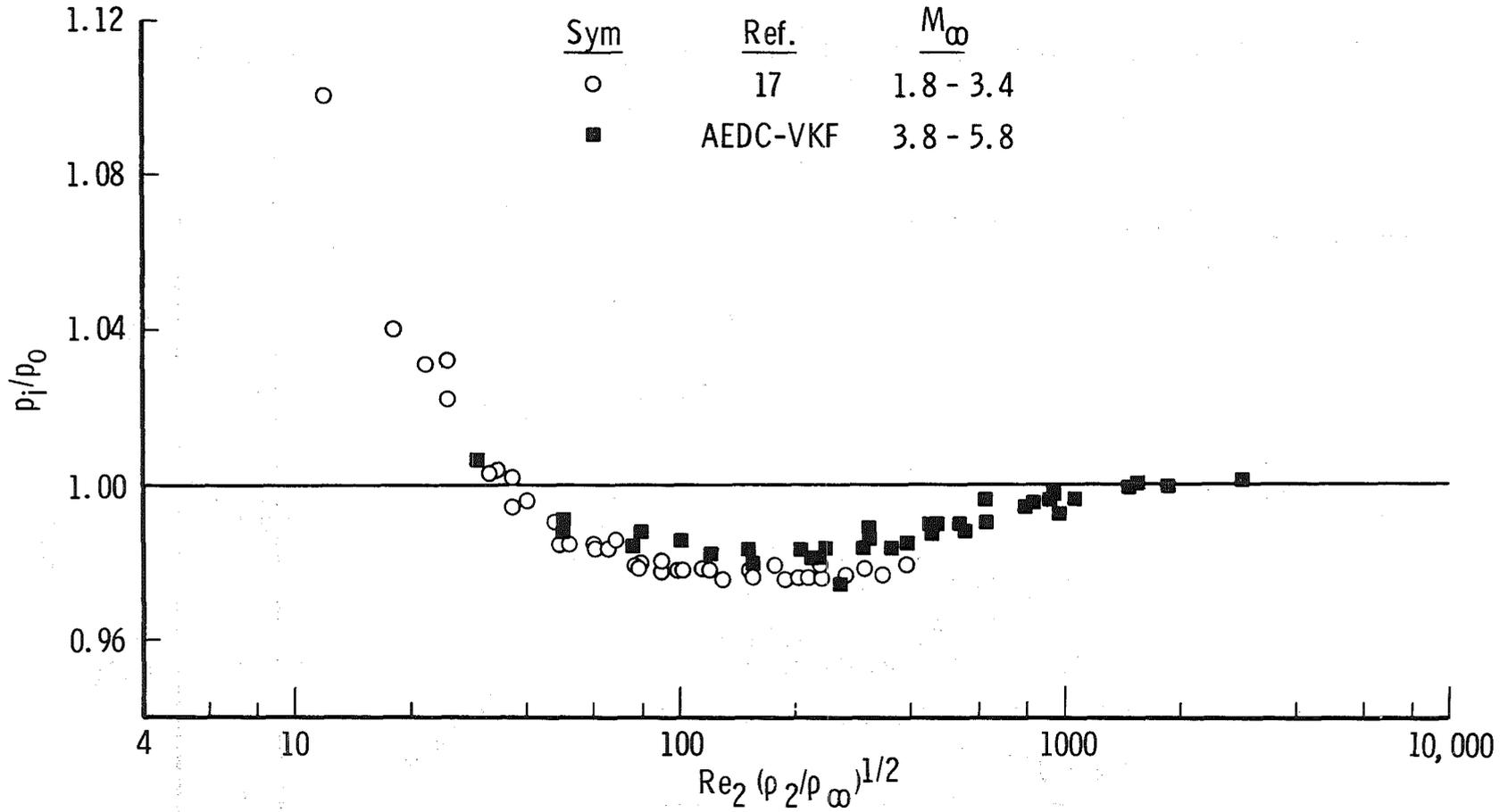
Fig. I-3 Comparison of AEDC-VKF Hemispherical-Nosed Probes with Sherman's Type A Source-Shaped Probes, $T_w = T_{aw}$
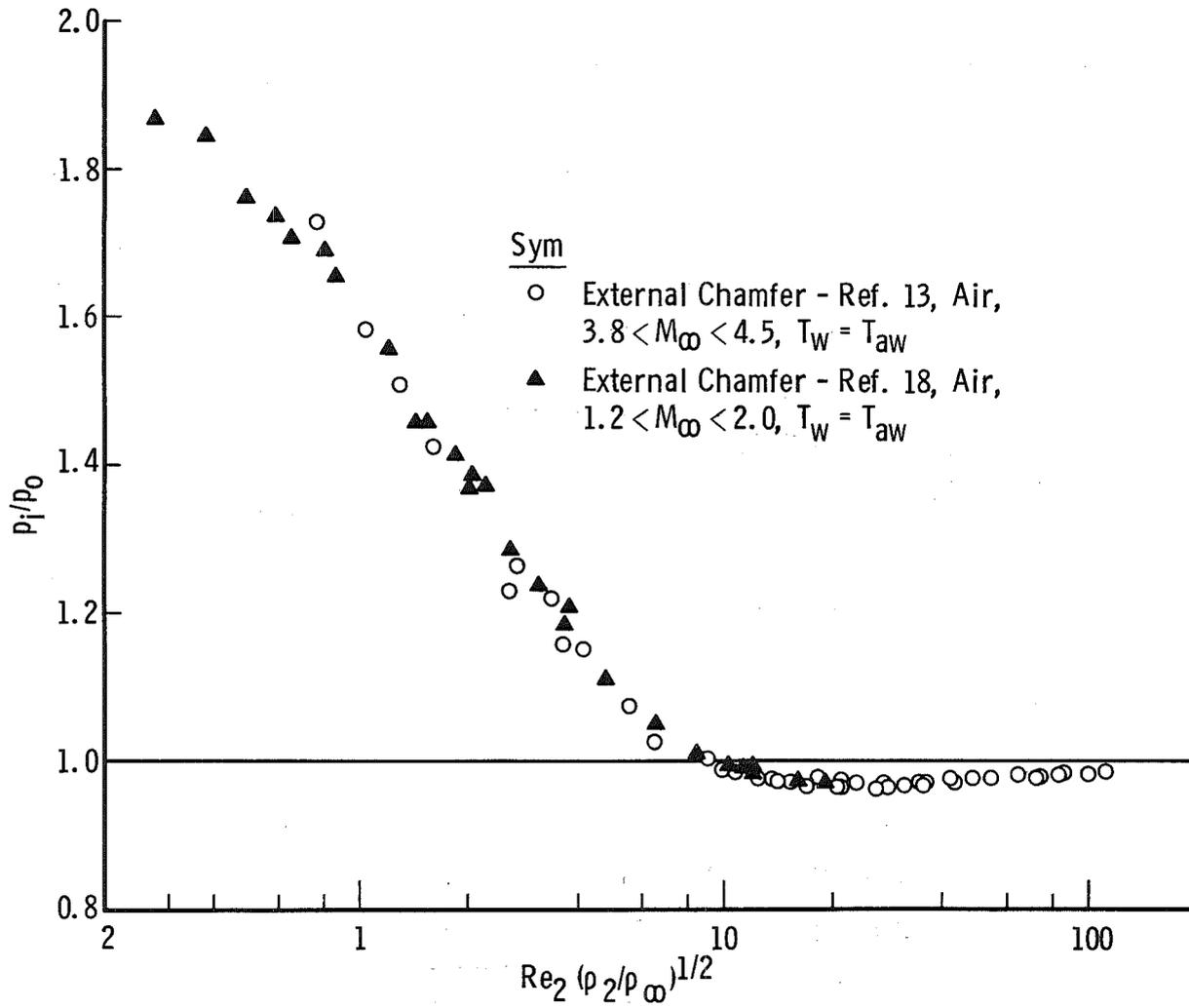
Fig. I-4 Result of Reinterpreting Enkenhus' Data by Forcing Its Agreement with Newer Data for Externally Chamfered Probes at Higher Reynolds Numbers

APPENDIX II

THE CHARACTERISTIC LENGTH

Figure II-1 shows the result of attempting to correlate data for hemispherical- and flat-nosed probes in nitrogen by using shock-layer thickness, Δ, instead of nose radius in defining Re_2. The shock-layer thicknesses used were the inviscid-flow values, which, for a typical Mach number of 4.7 in nitrogen, are

$$\Delta/R \text{ (hemisphere)} = 0.15$$

and

$$\Delta/R \text{ (flat-nose)} = 0.53$$

Inasmuch as shock radius of curvature and shock-layer thickness are in roughly the same ratio when comparing flat and hemispherical noses, the results shown in Fig. II-1 suggest that either Δ or R_S is a more characteristic length of the flow in this case.
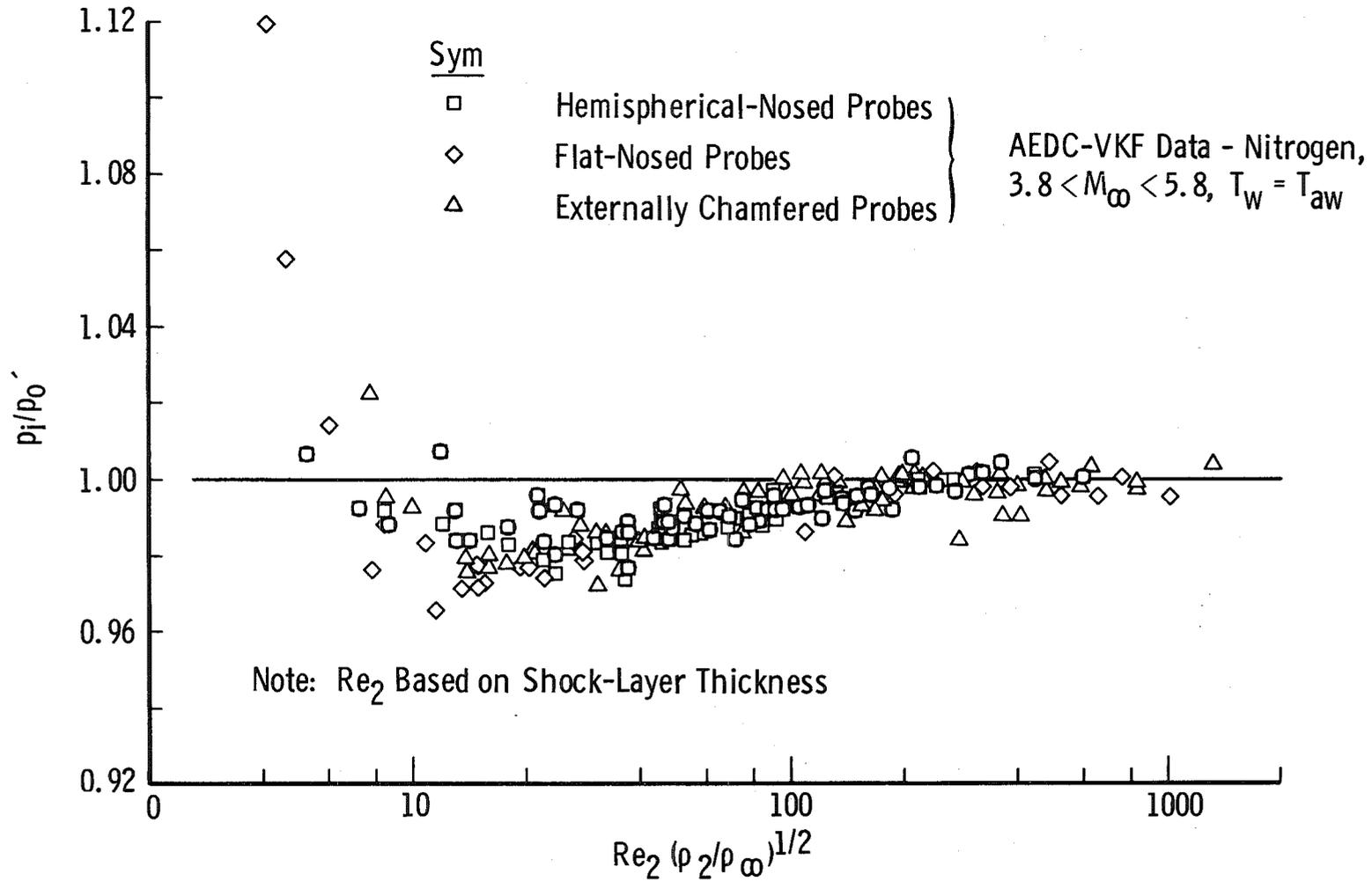
Fig. II-1 Comparison of Hemispherical, Flat-Nosed, and Externally Chamfered Probe Data on the Basis of Shock-Layer Thickness as Characteristic Length

TABLE 1

LDH TUNNEL OPERATING CONDITIONS WITH ARC-HEATER

	Nitrogen	Argon
Total pressure, psia	7.0-29.4	0.5-6.4
Total enthalpy, Btu/lb	740-2130	280-960
Total temperature, ^{o}K	1300-4000	1300-4260
Mach number	4.8-10.8	3.7-16.1
Unit Reynolds number, free stream, in.$^{-1}$	300-3500	270.0-4700
Unit Reynolds number behind normal shock, in.$^{-1}$	35.0-1140	14.0-1080
Mean free path, free stream, billiard-ball gas model, in.	0.002-0.058	0.002-0.057
Uniform flow core diameter at test section, in.	0.2-1.2	0.5-1.5

TABLE 2

LDH TUNNEL OPERATING CONDITIONS WITHOUT ARC-HEATER

|	Nitrogen	Argon and Helium
Total pressure, psia	0.06-2.7	0.08-3.0
Total enthalpy, Btu/lb	140	70
Total temperature, $^{\circ}$K	300	300
Mach number	3.8-5.8	4.0-8.0
Unit Reynolds number, free stream, in.$^{-1}$	620-15,000	1600-50,000
Unit Reynolds number behind normal shock, in.$^{-1}$	190-3500	264-3800
Mean free path, free stream, billiard-ball gas model, in.	0.0005-0.012	0.0001-0.006
Uniform flow core diameter at test section, in.	0.8-1.5	0.5-1.0

TABLE 3

DIMENSIONS OF RADIATION-COOLED PROBES
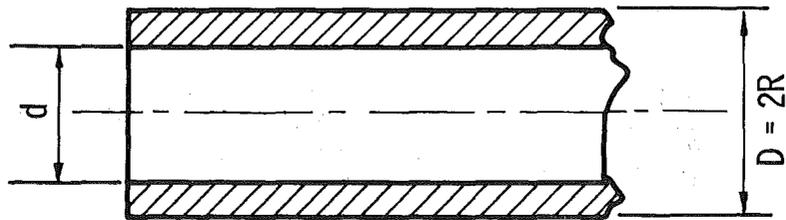
Flat-Nosed Probe
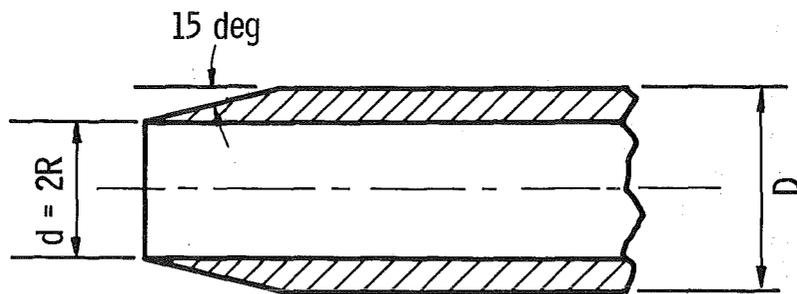
Externally Chamfered Probe

D, in.	d, in.	Flat-Nosed	Externally Chamfered	
0.75	0.625	X	X	
0.625	0.436	X		
0.50	0.335	X	X	
0.375	0.300	X	X	
0.250	0.182	X	X	
0.188	0.147	X	X	
0.156	0.116	X		$0.51 < d/D < 0.83$
0.125	0.081		X	
0.125	0.063		X	
0.086	0.066	X		
0.060	0.050		X	
0.060	0.032		X	
0.035	0.024	X		
0.125	0.092	X	X	

TABLE 4

DIMENSIONS OF WATER-COOLED PROBES
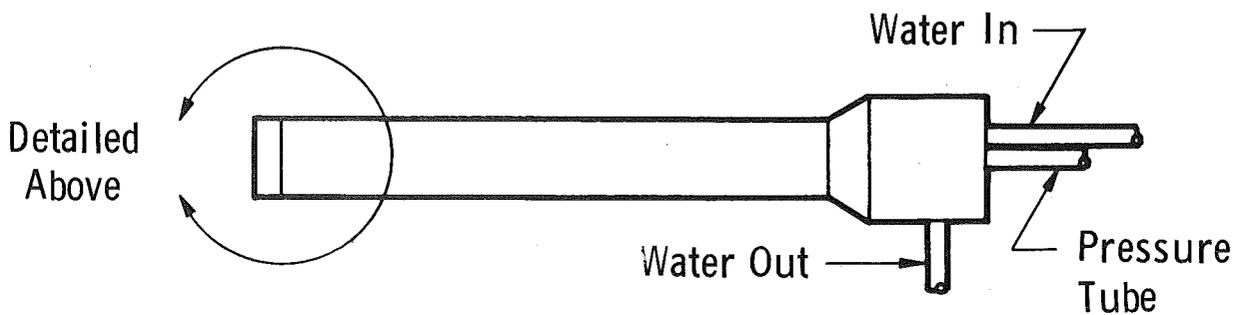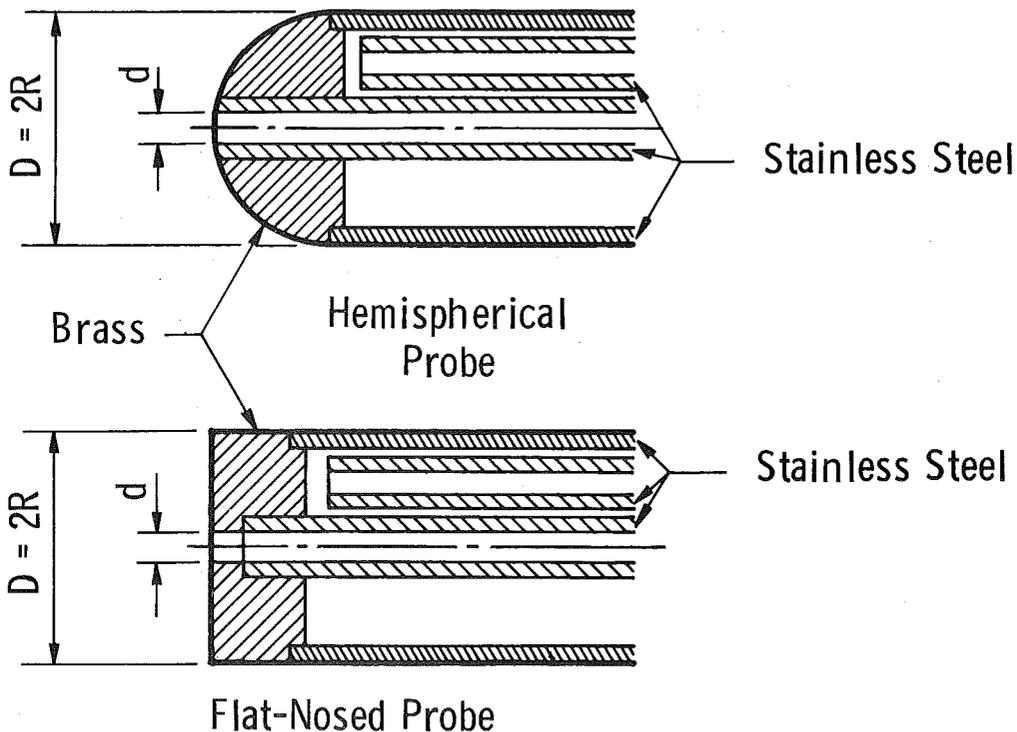
D, in.	d, in.	Flat-Nosed	Hemi-Spherical
1.00	0.150		X
0.75	0.116	X	X
0.50	0.075	X	X
0.375	0.065		X
0.250	0.035	X	X
0.150	0.015		X
0.125	0.085	X	

$d/D \simeq 0.15$
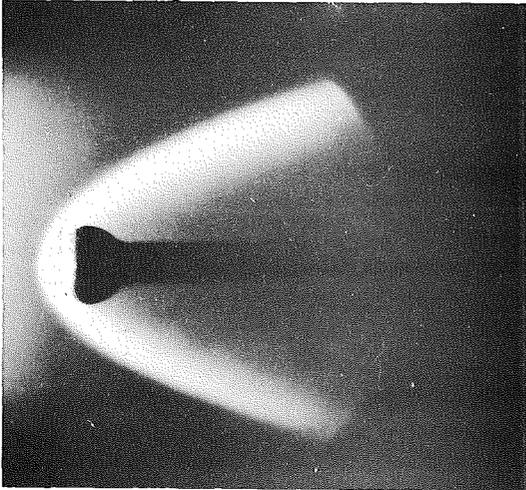
M_∞	4.7
T_0	2780^0K
$Re_2/in.$	210
R	0.125 in.
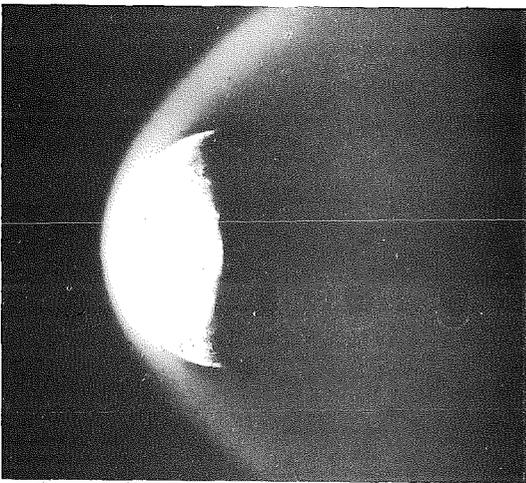
M_∞	6.2
T_0	2990^0K
$Re_2/in.$	330
R	0.344 in.
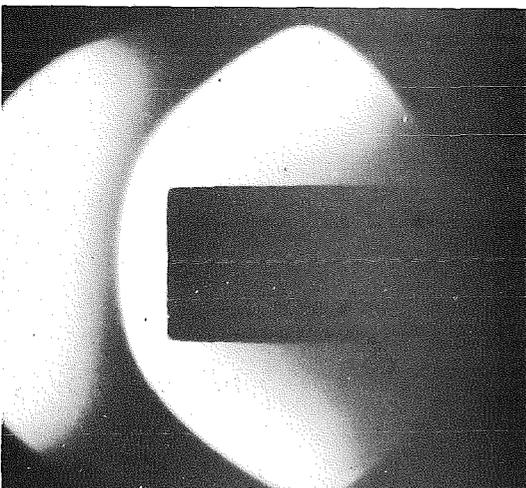
M_∞	4.7
T_0	2780^0K
$Re_2/in.$	210
R	0.249 in.

Fig. 1 Flow over Spheres and Flat-Nosed Bodies in Argon
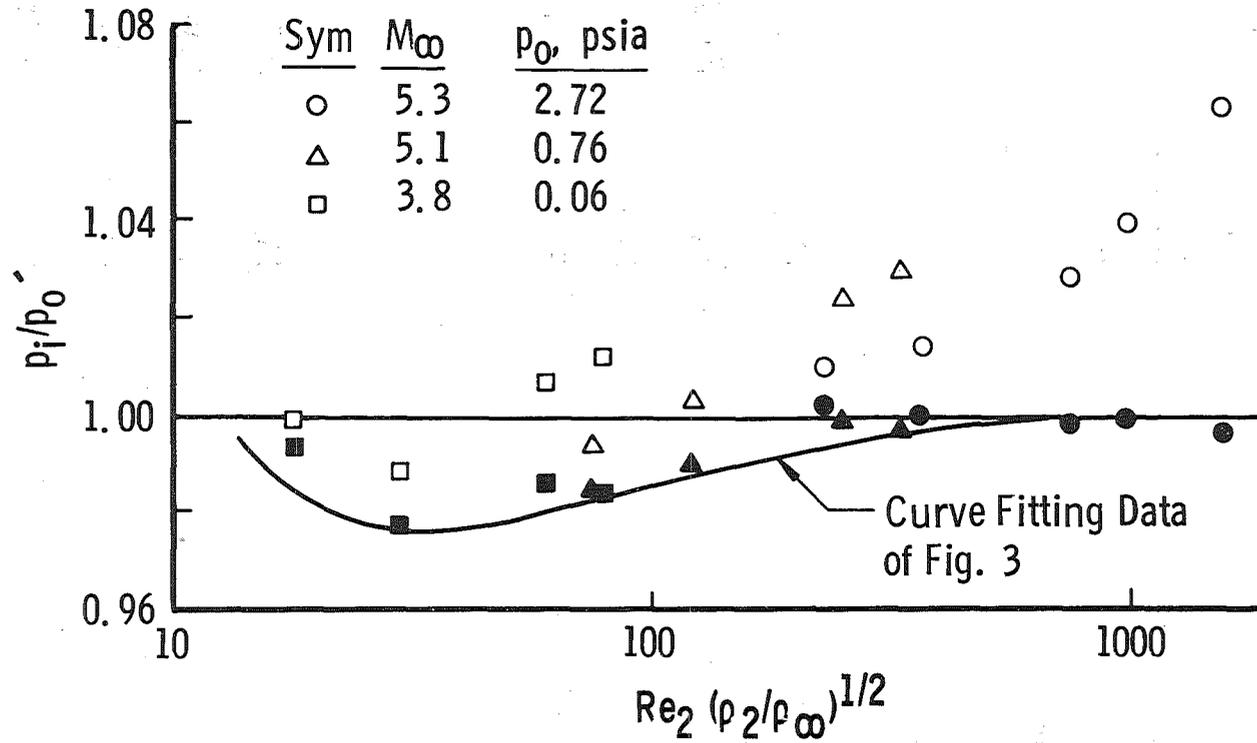
Fig. 2 Example of the Effect of Correcting for Axial Pressure Gradients with $T_w = T_{aw}$
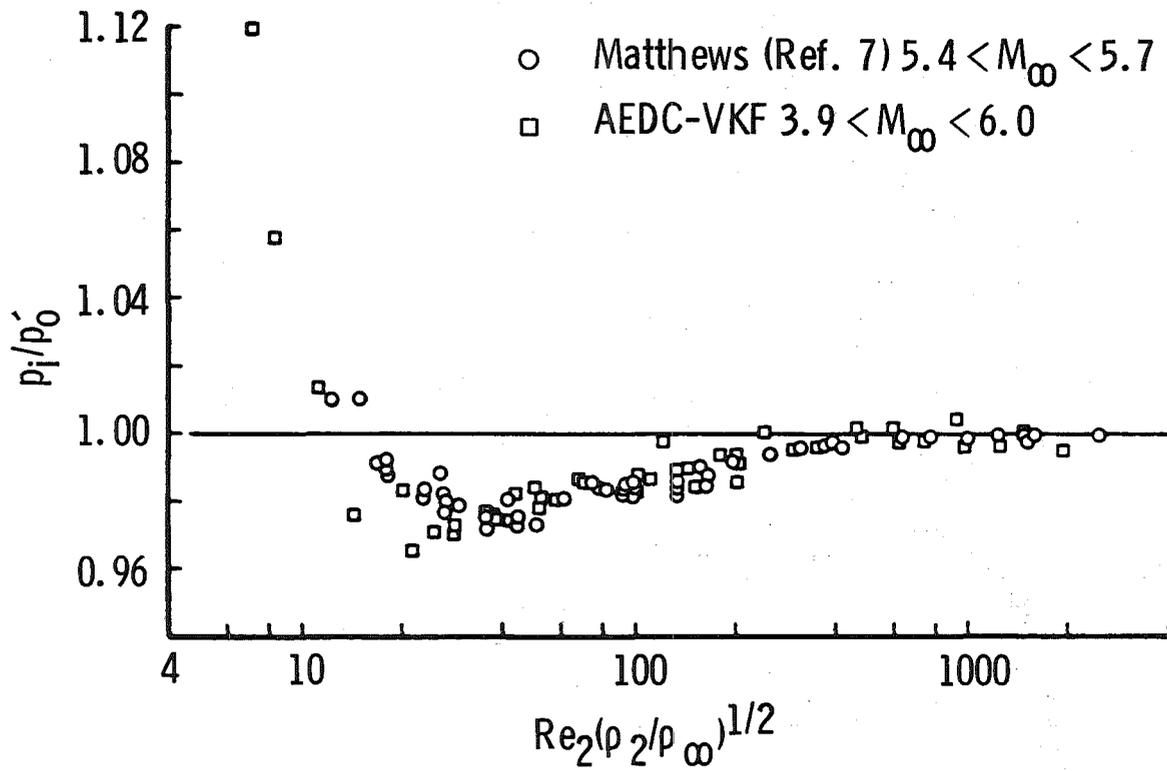
Fig. 3 Comparison of AEDC-VKF and GALCIT Data for Flat-Nosed Probes in Nitrogen and Air, Respectively, with $T_w = T_{aw}$

Axisymmetric Body

Shock

y

R

x

(2)

(∞)

(w)

R_S
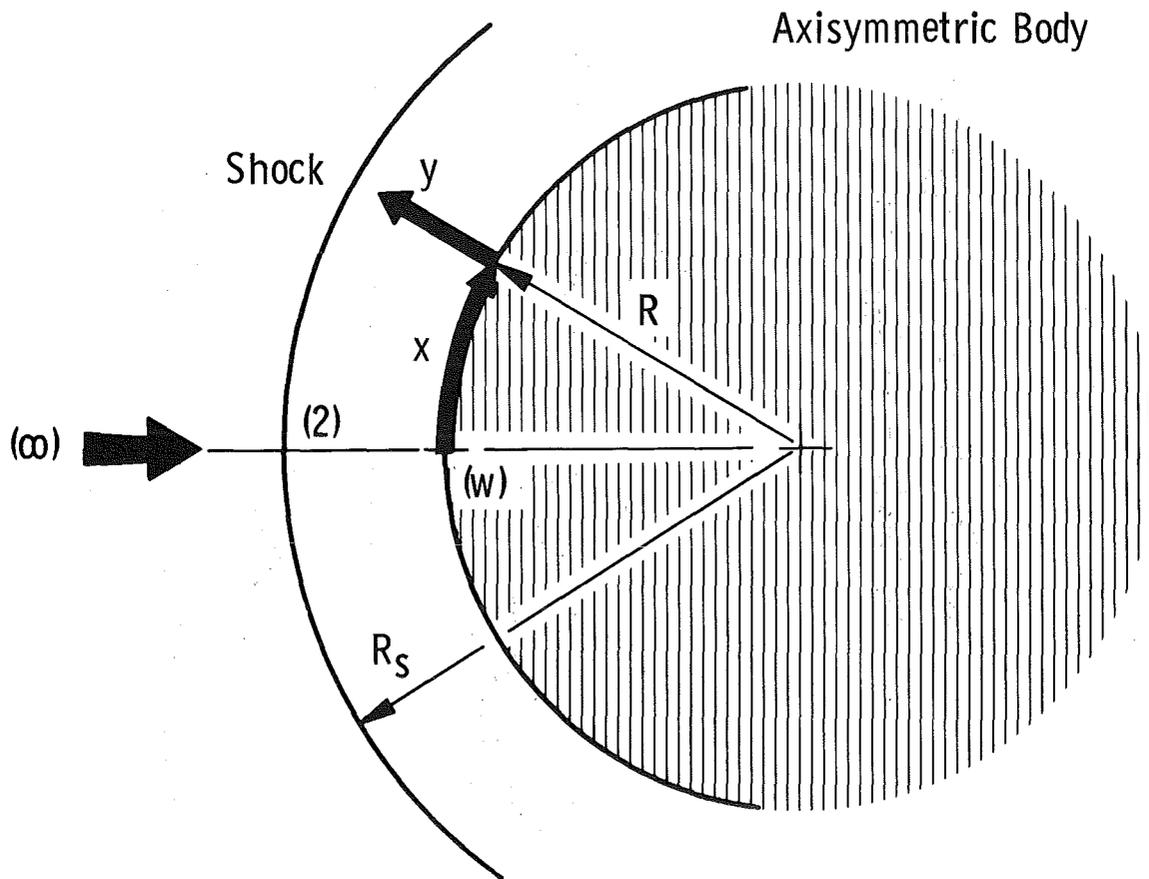
Fig. 4 Nomenclature and Coordinate System
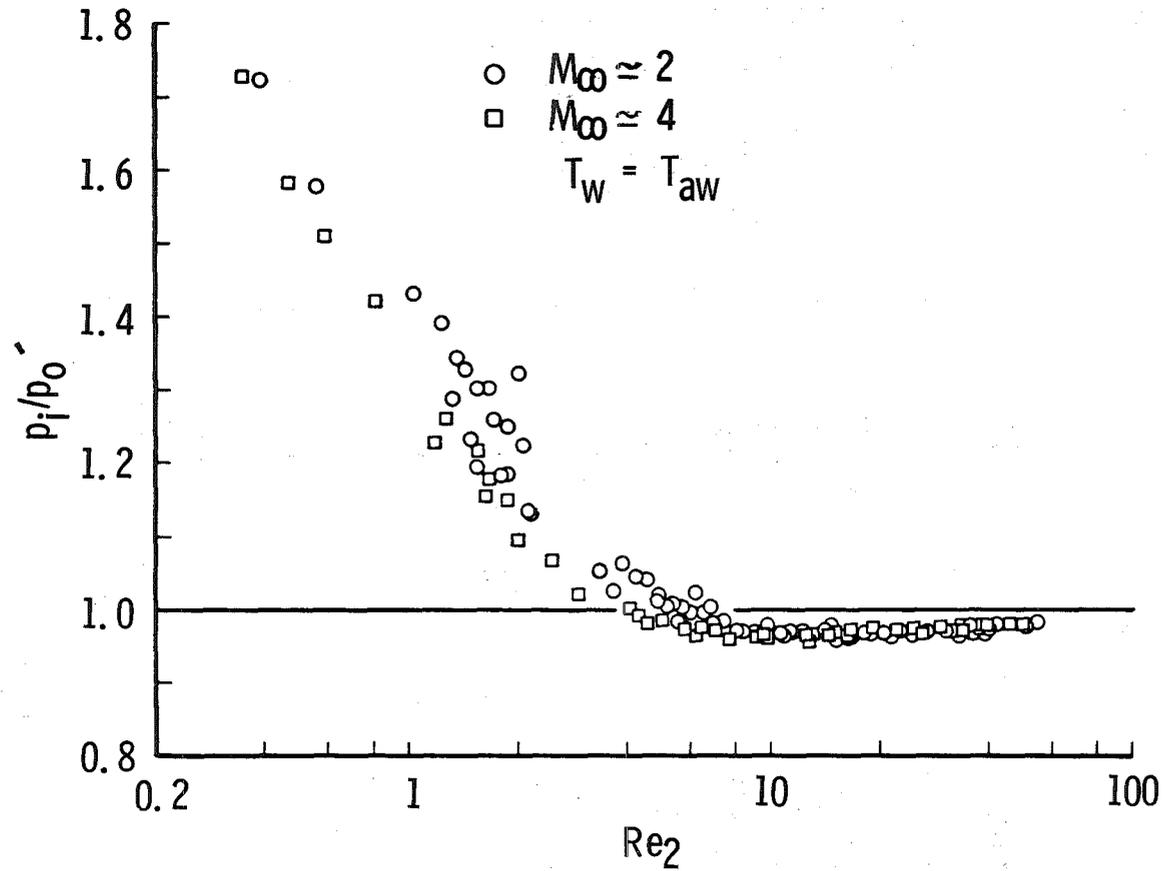
Fig. 5 Data of Ashkenas for Flat-Nosed, Externally Chamfered Probes (Ref. 13) Correlated by
Re₂ with T_w = T_aw
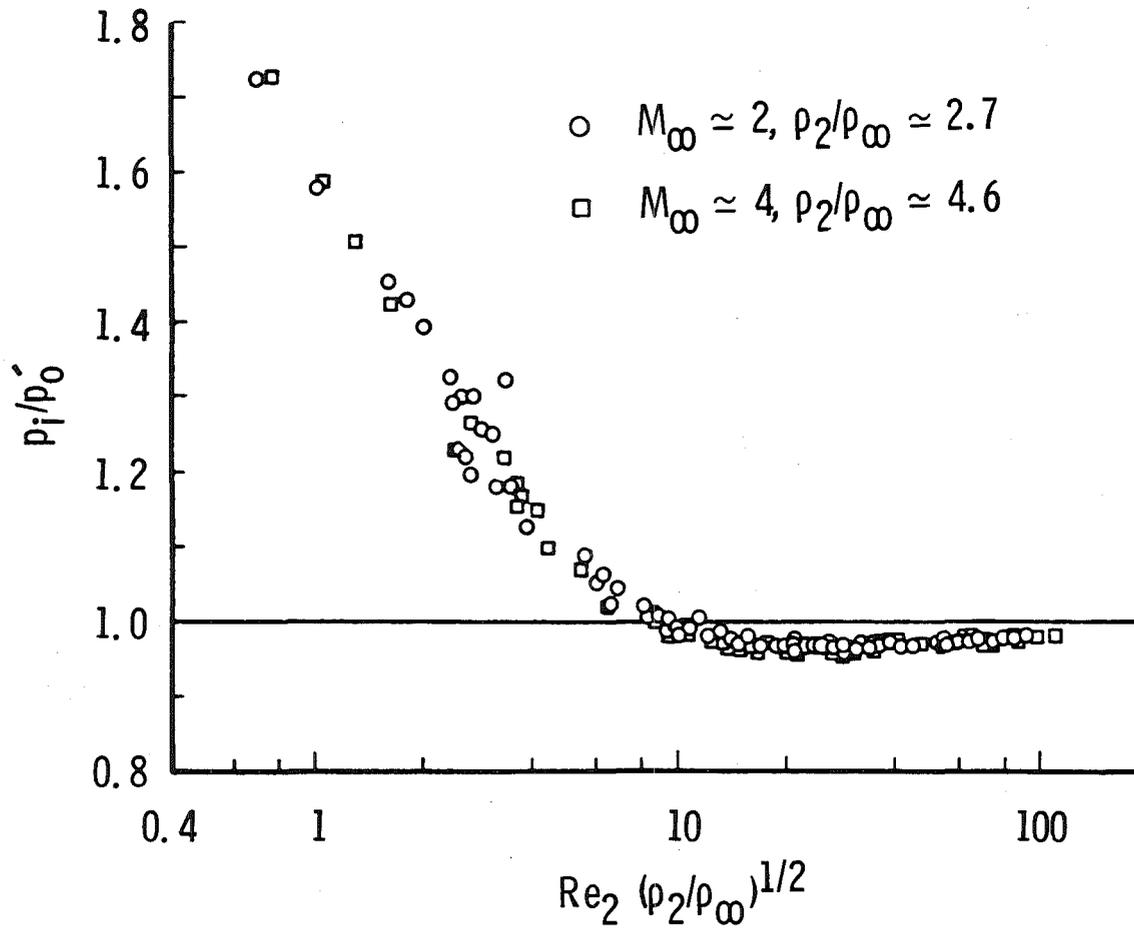
Fig. 6 Data of Ashkenas for Flat-Nosed, Externally Chamfered Probes (Ref. 13) Correlated by $Re_2 (\rho_2/\rho_\infty)^{1/2}$ with $T_w = T_{aw}$

Sym	M_∞	$Re_2 \, (\rho_2/\rho_\infty)^{1/2}$, in.$^{-1}$	
○	6.1	4480	
□	7.2	2940	
◇	5.8	2400	
◿	6.6	1680	Argon
△	7.3	1280	
⬡	5.6	1720	
⬯	7.1	920	
☆	5.1	500	
▲	4.3	1220	
●	5.1	790	Helium
■	5.7	594	

Curve Fitting Data of Fig. 3 for Flat-Nosed Probe in Nitrogen with $T_w = T_{aw}$

p_i/p_0'

$Re_2 \, (\rho_2/\rho_\infty)^{1/2}$
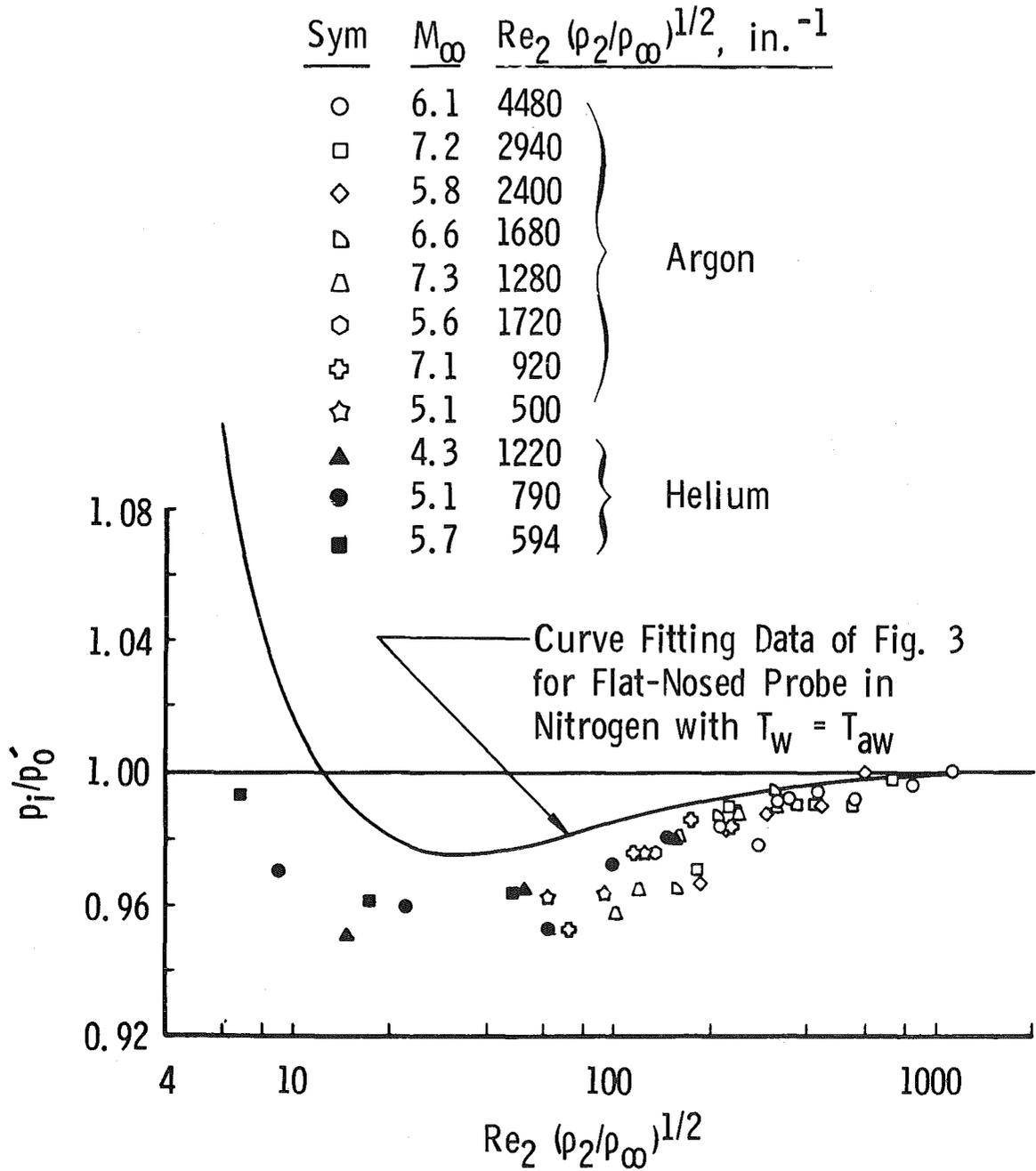
Fig. 7 AEDC-VKF Data for Flat-Nosed Probes in Argon and Helium with $T_w = T_{aw}$

Sym	M_∞	$Re_2(\rho_2/\rho_\infty)^{1/2}$ in.$^{-1}$
○	4.7	7810
●	5.3	4570
◑	5.8	3510
□	4.7	4430
▪	5.2	2870
◨	5.6	2110
◇	4.6	2450
◆	5.1	1670
◈	5.4	1260
▷	4.4	1180
◐	4.8	832
◭	5.2	640
△	3.8	401

Curve Fitting Data of Fig. 3 for Flat-Nosed Probe in Nitrogen with $T_w = T_{aw}$
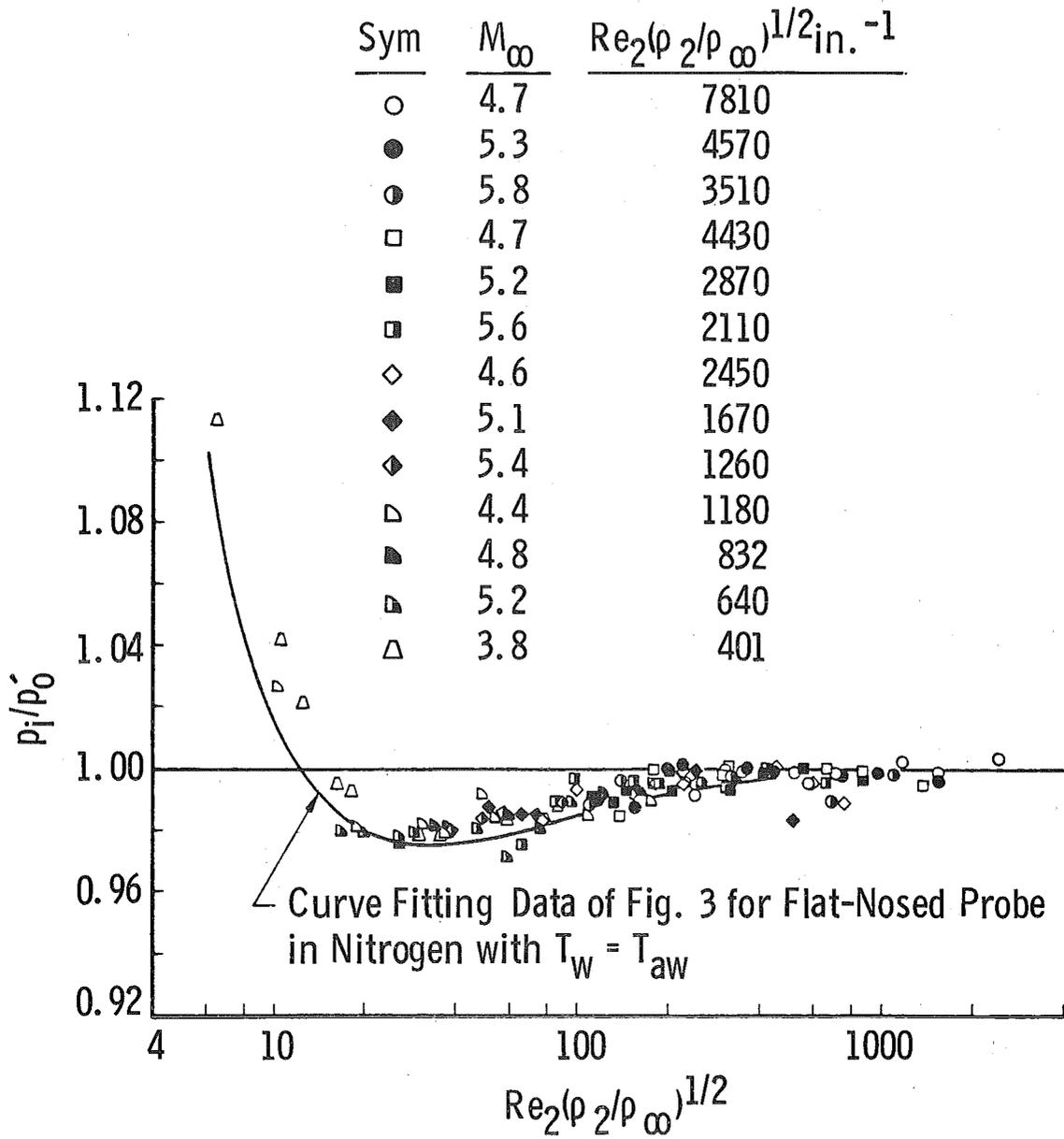
Fig. 8 AEDC-VKF Data for Externally Chamfered Probes in Nitrogen with $T_w = T_{aw}$

36

| Sym	M_∞	$Re_2 \, (\rho_2/\rho_\infty)^{1/2}$, in.$^{-1}$
○	4.7	7810
●	5.3	4570
◐	5.8	3510
□	4.7	4430
■	5.2	2870
◙	5.6	2110
◇	4.6	2440
◆	5.1	1670
◈	5.4	1250
◭	4.4	1180
◩	4.8	830
◪	5.2	640
△	3.8	410
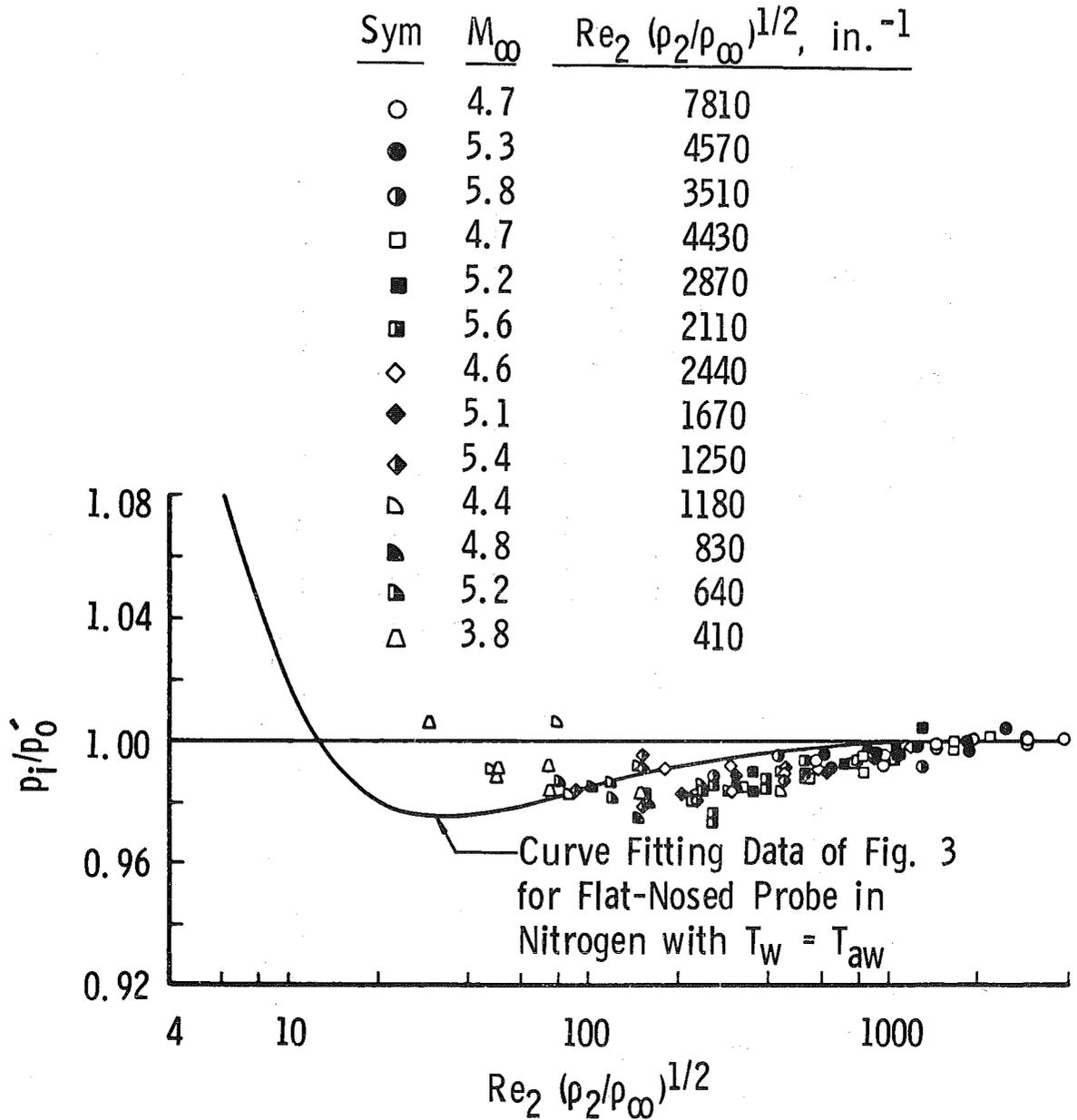
Fig. 9 AEDC-VKF Data for Hemispherical-Nosed Probes in Nitrogen with $T_w = T_{aw}$

37
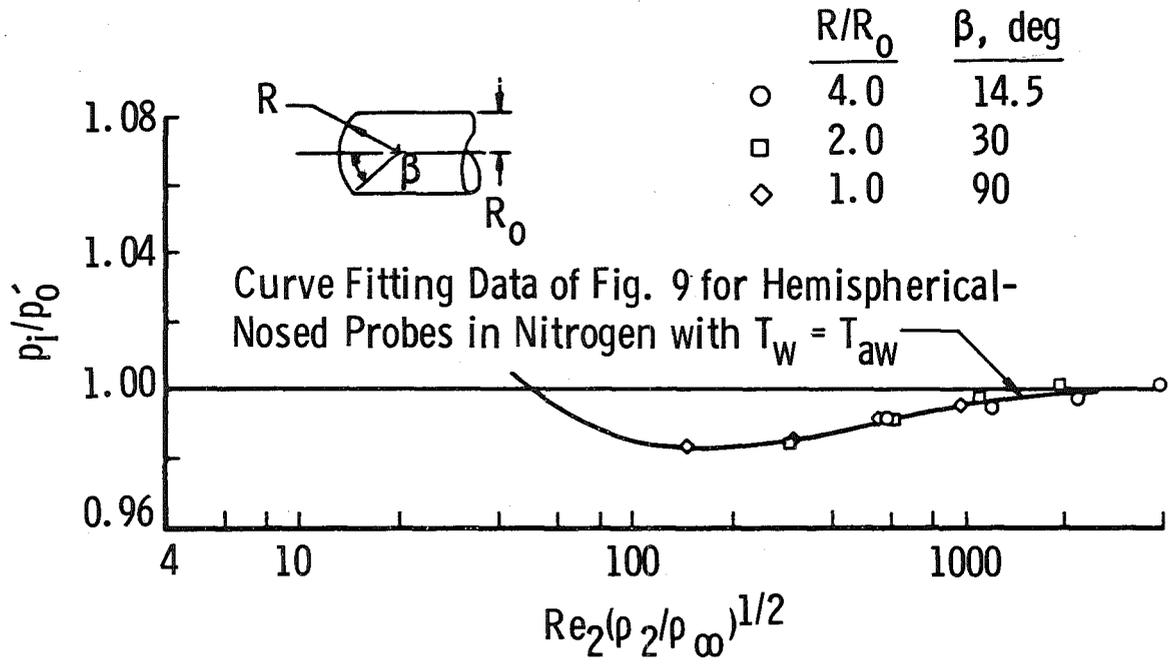
Fig. 10 AEDC-VKF Data for "Incomplete" Hemispherical-Nosed Probes in Nitrogen with
$T_w = T_{aw}$ and $4.4 < M_\infty < 4.7$

Sym	M_∞	$Re_2\ (\rho_2/\rho_\infty)^{1/2}$, in.$^{-1}$
△	6.2	7300
○	6.1	4480
□	5.7	2400
◇	7.3	1280
◁	5.6	1720

Curve Fitting Data of Fig. 9 for Hemispherical-Nosed Probe in Nitrogen with $T_W = T_{aw}$

Curve Fitting Data of Fig. 7 for Flat-Nosed Probe in Argon with $T_W = T_{aw}$

Theory of Levinsky and Yoshihara (Ref. 15)

y-axis: p_i/p_0' — 1.08, 1.04, 1.00, 0.96, 0.92

x-axis: $Re_2\ (\rho_2/\rho_\infty)^{1/2}$ — 10, 100, 1000
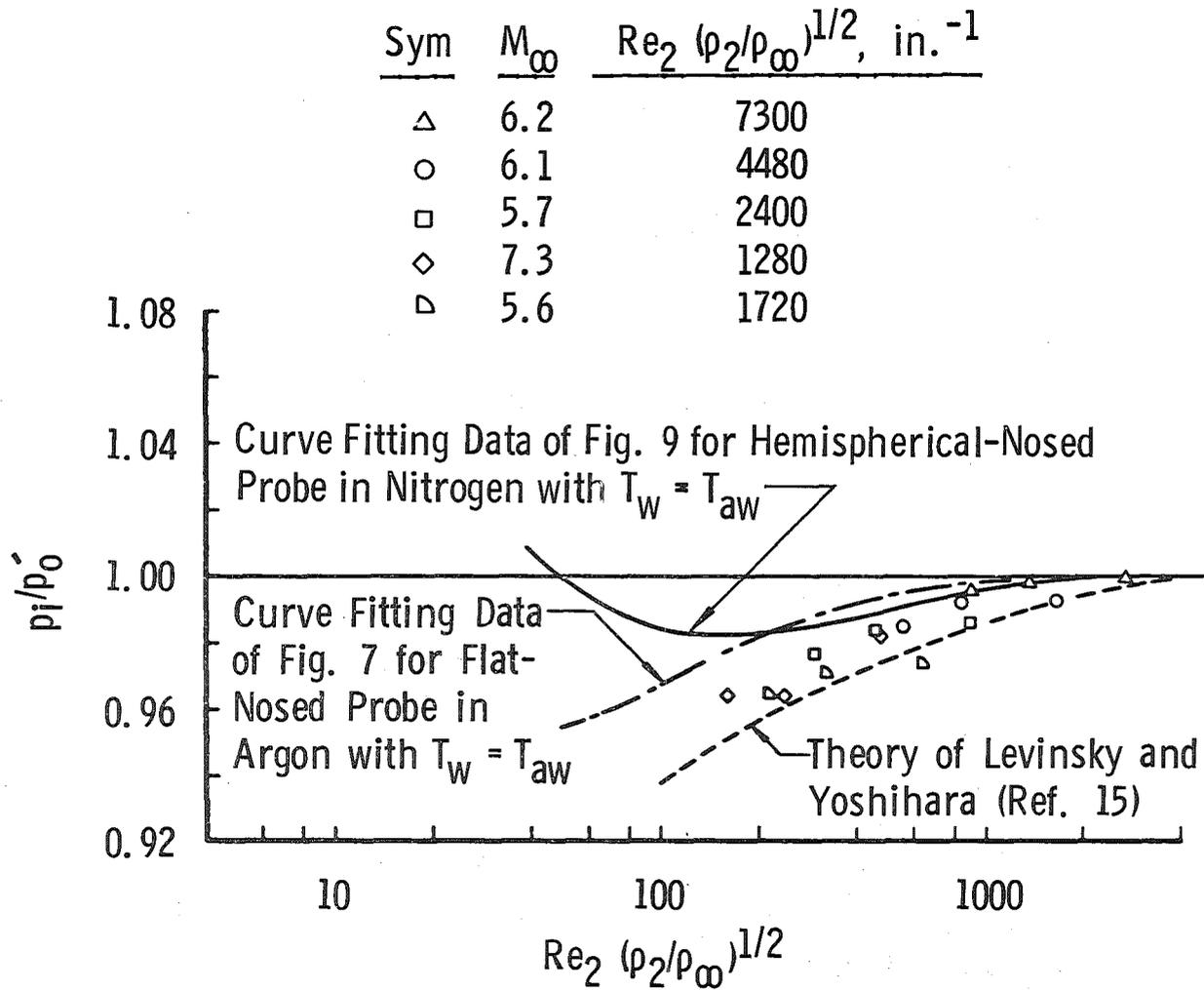
Fig. 11 AEDC-VKF Data for Hemispherical-Nosed Probes in Argon with $T_w = T_{aw}$

Sym	M_∞	T_0, °K	$Re_2(\rho_2/\rho_\infty)^{1/2}$ in. $^{-1}$
○	7.0	1490	1030
□	8.3	1490	482
△	9.2	1490	302
◇	7.0	2600	485
▽	7.2	1915	1110
▽	6.8	2300	400
○	7.2	2300	630
●	10.7	3000	91
■	9.3	2240	306
⬣	9.1	2070	250
▼	9.7	2070	281
◢	8.8	2070	420

Curve Fitting Data of Fig. 3 for Flat-Nosed Probe in Nitrogen with $T_w = T_{aw}$
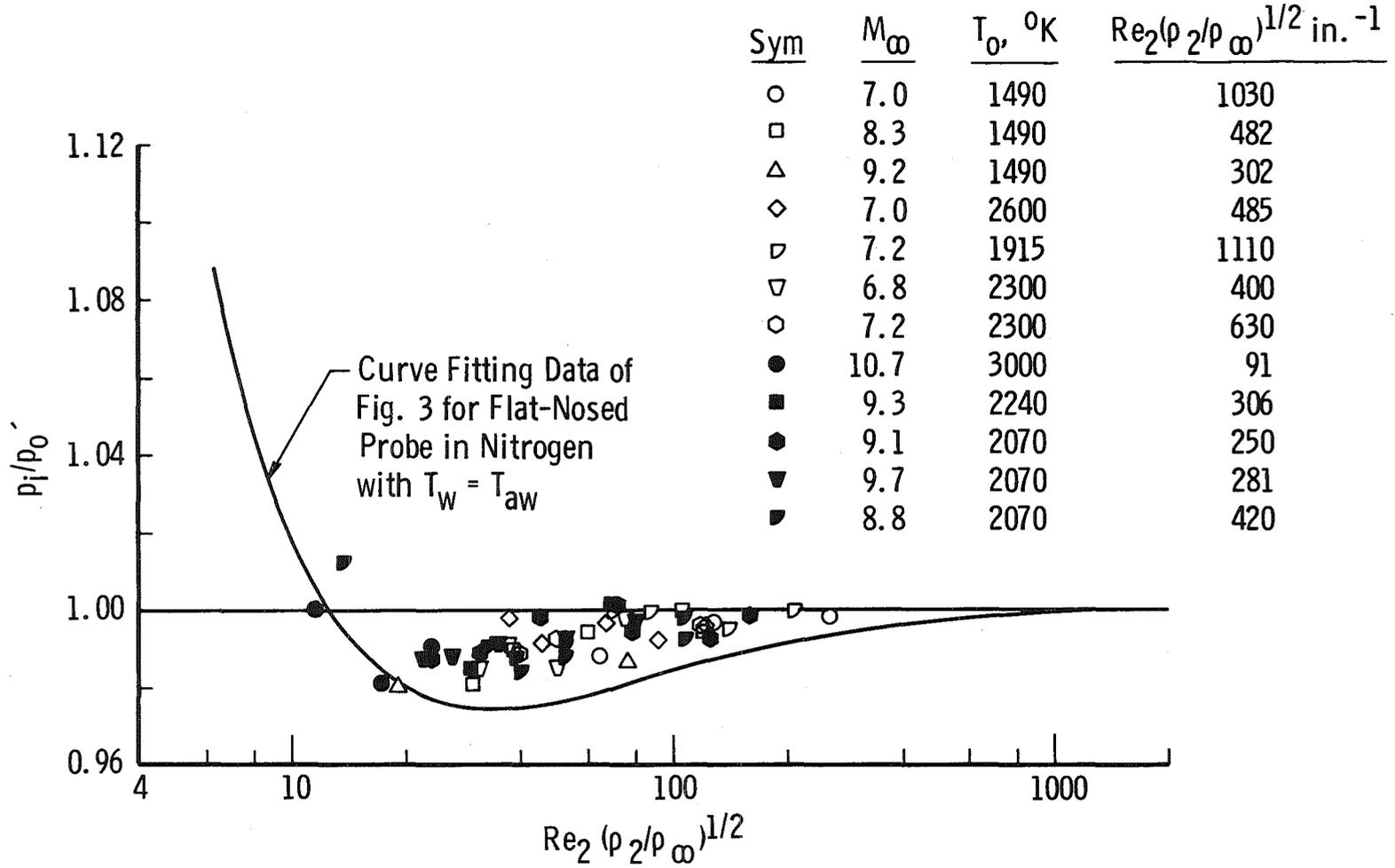
Fig. 12 AEDC-VKF Data for Flat-Nosed Probes in Nitrogen with $T_w = 0.2$ to $0.3\ T_0$

| Sym	M_∞	T_0, °K	$Re_2(\rho_2/\rho_\infty)^{1/2}$ in. $^{-1}$
○	4.0	1500	1640
□	4.7	1500	1180
◇	7.0	1500	390
◁	3.9	2780	630
△	4.4	2780	450
⬠	6.7	2780	160
✪	3.7	2590	330
⬮	4.3	2590	240
●	3.9	1310	1960
◼	3.8	2180	680
◆	4.2	2780	510
◖	5.3	2780	290
✚	6.4	2780	180
▲	4.5	2890	810
⬣	5.6	2890	490
▼	7.1	2890	260

Curve Fitting Data of Fig. 7 for Flat-Nosed Probe in Argon with $T_W = T_{aw}$

Curve Fitting Data of Fig. 12 for Flat-Nosed Probe in Nitrogen with $T_W < T_0$
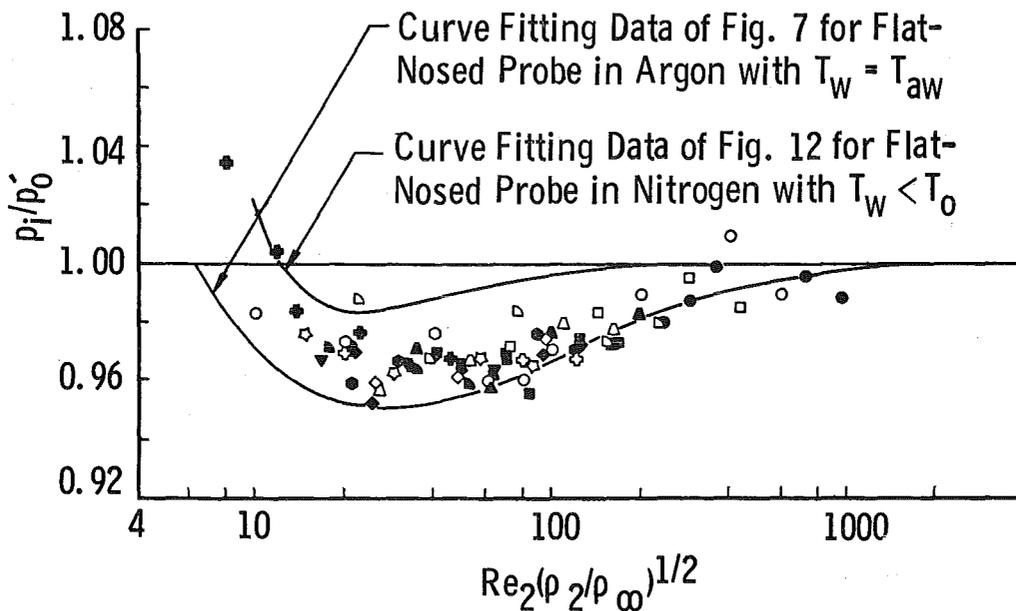
Fig. 13 AEDC-VKF Data for Flat-Nosed Probes in Argon with T_W = 0.1 to 0.3 T_0

Sym	M_∞	$T_0,\ {}^\circ K$	$Re_2(\rho_2/\rho_\infty)^{1/2}$
○	7.0	1490	1030
□	8.3	1490	480
◇	9.2	1490	300
△	4.8	1530	2540

Curve FittingData of Fig. 12 for a Flat-Nosed Probe in Nitrogen with $T_w < T_{aw}$

Curve Fitting Data of Fig. 9 for Hemispherical-Nosed Probe in Nitrogen with $T_w = T_{aw}$

p_i/p_0'
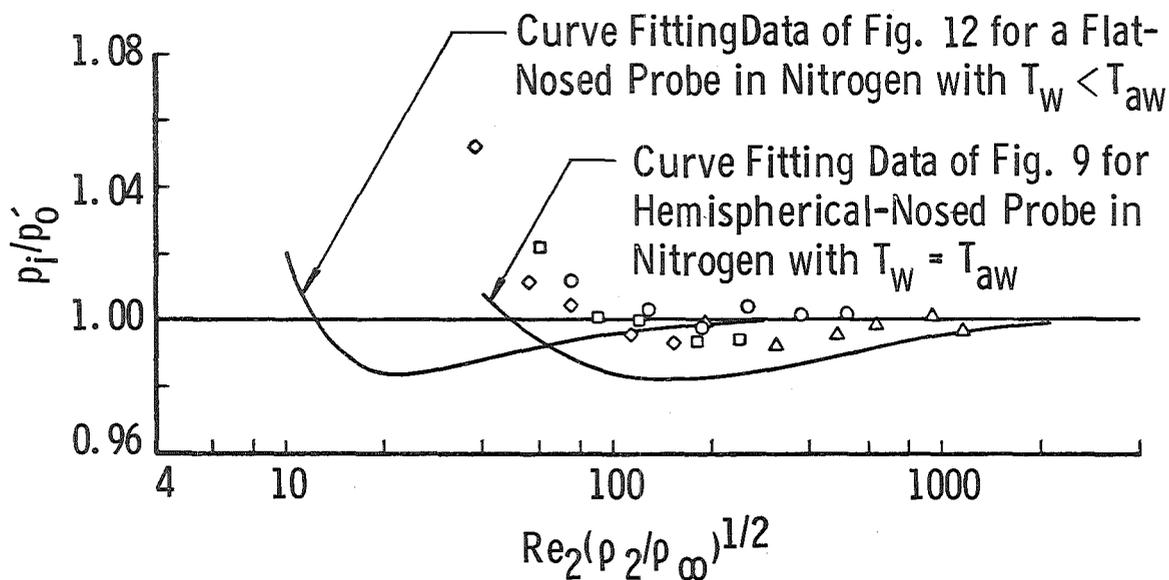
$Re_2(\rho_2/\rho_\infty)^{1/2}$

Fig. 14 AEDC-VKF Data for Hemispherical-Nosed Probes in Nitrogen with $T_w = 0.2\ T_0$

Sym	M_∞	T_0, °K	$Re_2(\rho_2/\rho_\infty)^{1/2}$in.$^{-1}$
○	4.6	2730	790
□	5.9	2730	437
◇	7.0	2730	246
▽	4.4	2780	446
▽	5.6	2780	262
○	6.7	2780	164
✧	4.6	1500	1180
☆	5.9	1500	635
△	7.0	1500	390
○	4.5	1500	622
▽	5.7	1500	350
△	6.8	1500	226
●	4.3	2580	236
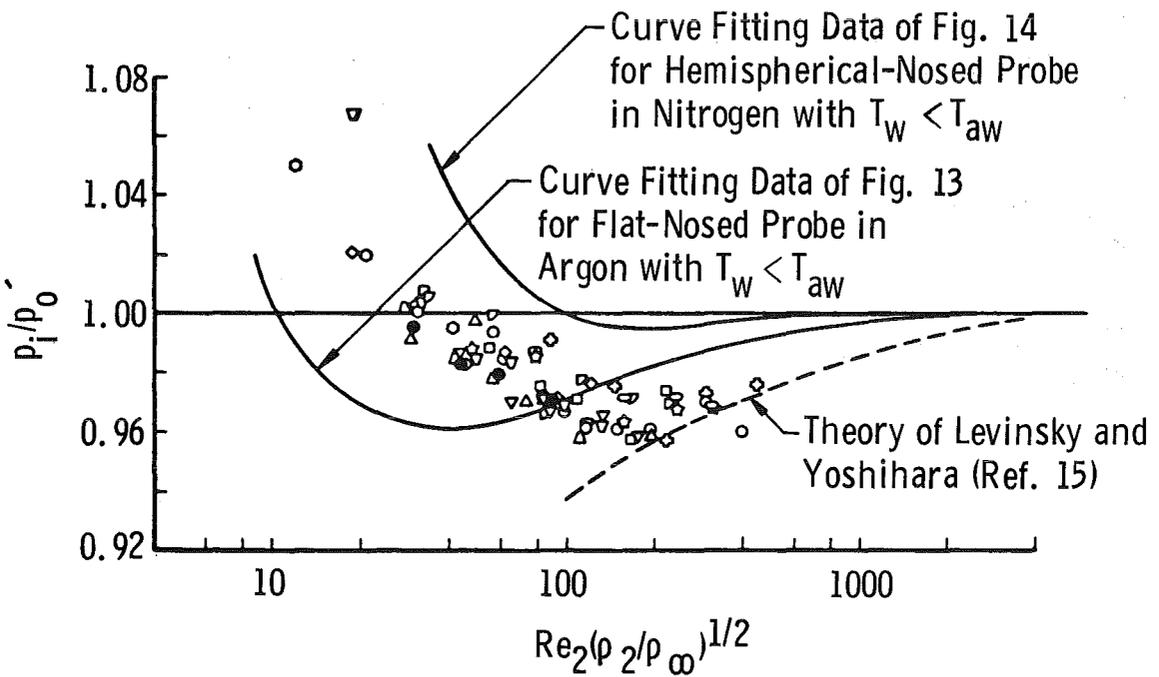
Fig. 15 AEDC-VKF Data for Hemispherical-Nosed Probes in Argon with T_w = 0.1 to 0.2 T_0
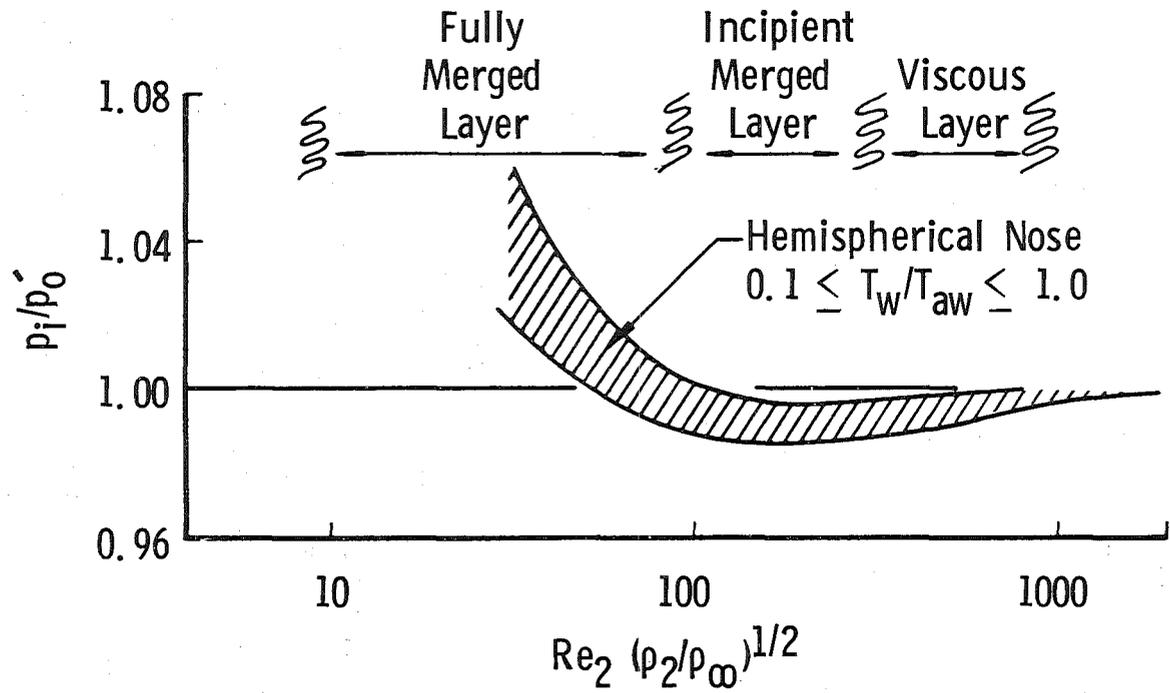
Fig. 16 An Example of the Relation between Impact Pressure and Probstein's Regimes of Rarefied Flow
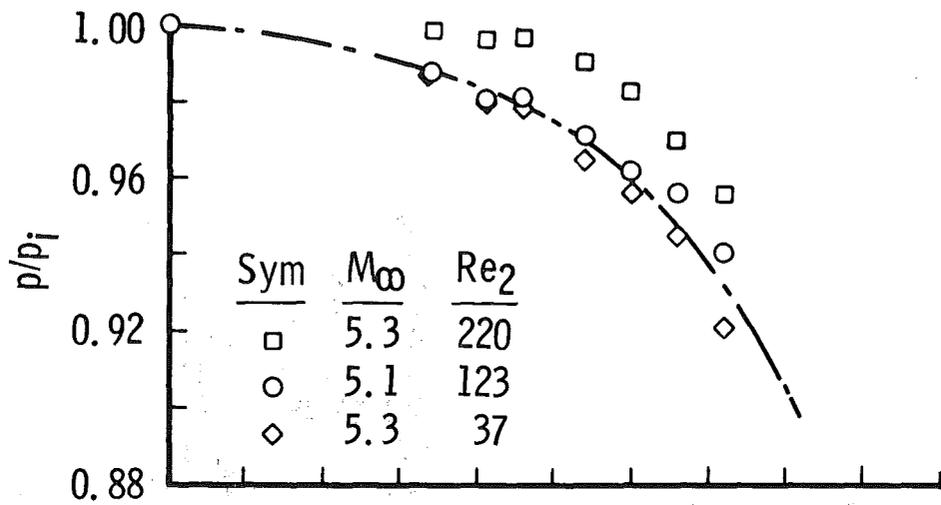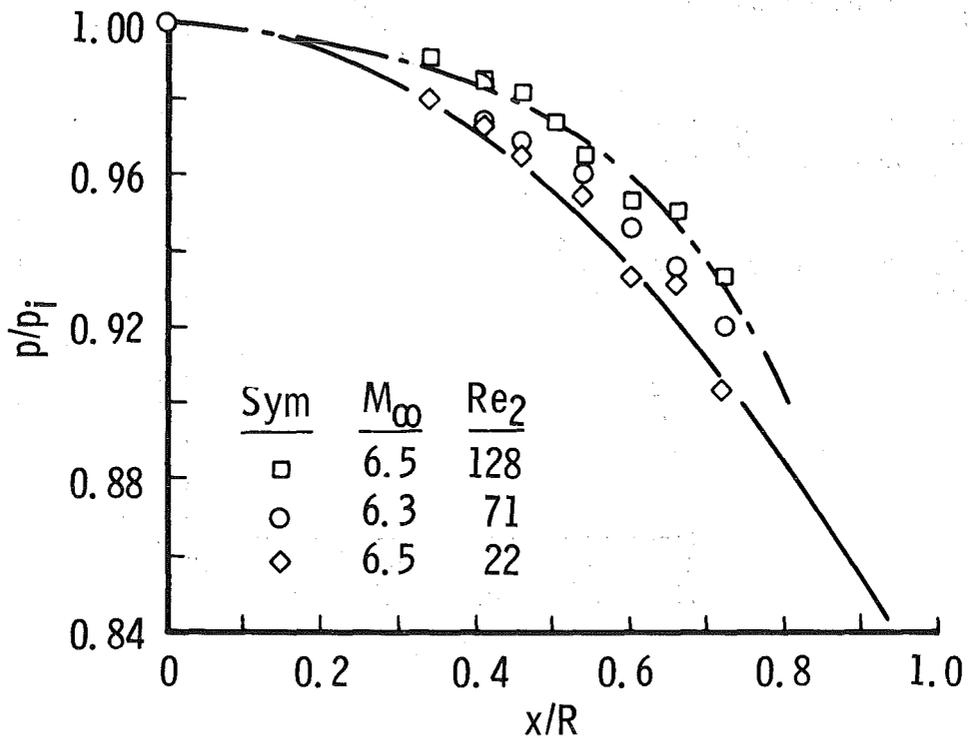
Fig. 17 Pressure Distribution on a Flat Nose in Argon with $T_w \simeq 0.15\ T_o$

Sym	M_∞	Re_2	T_0, $^\circ K$
○	6.3	93	3090
□	6.0	86	1940
△	6.0	63	3150
◇	6.0	56	3640
◿	5.4	28	4020
⬡	6.1	45	3180

Modified Newtonian

$M_\infty = 5.4$

$M_\infty = 6.3$
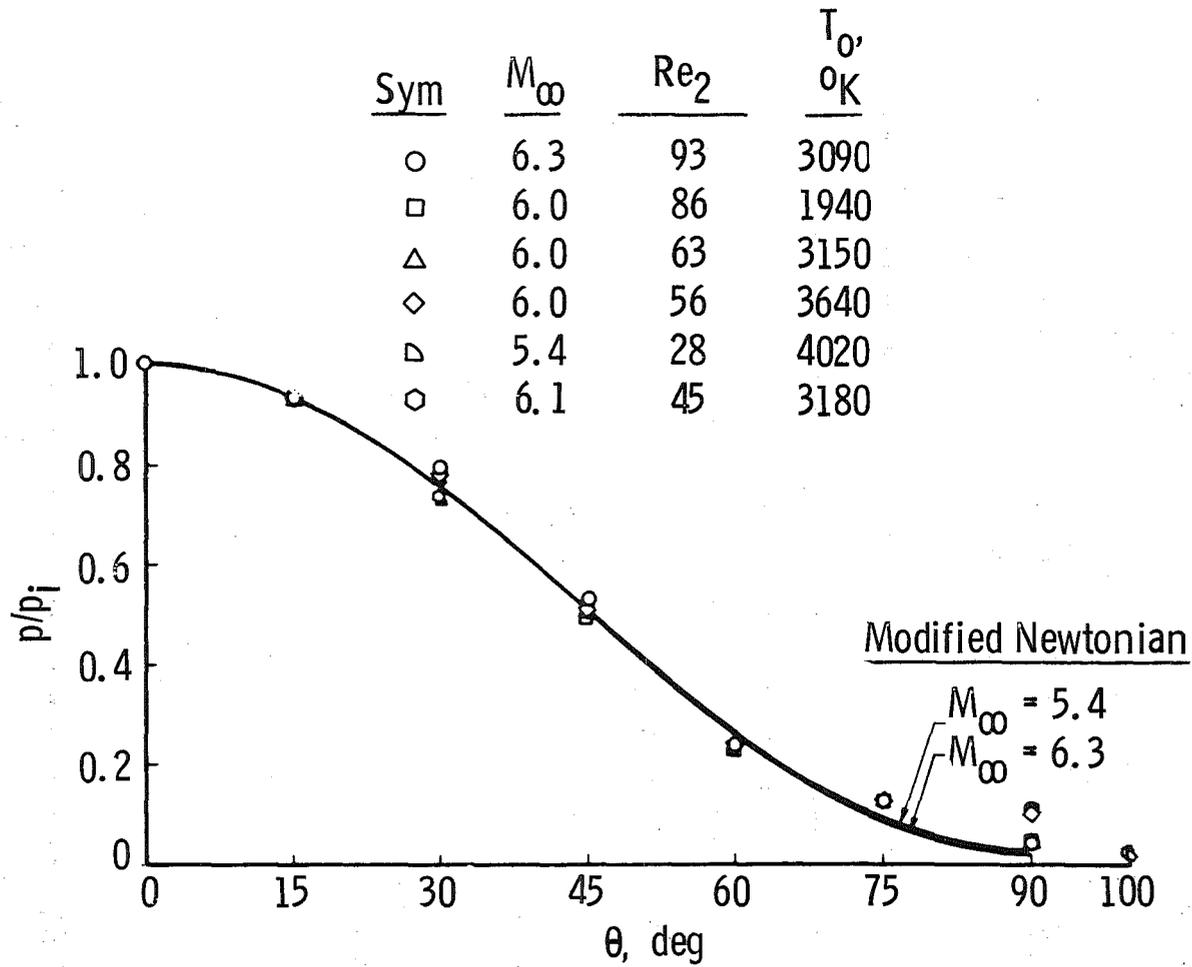
Fig. 18 Pressure Distribution on a Hemispherical Nose in Argon with $T_w \cong 0.1\ T_0$